Exploring different thermoplastics from lignocellulosic building blocks and monomers

Bonjour, Olivier

2023

Document Version:
Publisher's PDF, also known as Version of record

Green Chemistry

PAPER

View Article Online
View Journal | View Issue

Cite this: *Green Chem.*, 2020, **22**, 3940

Rigid biobased polycarbonates with good processability based on a spirocyclic diol derived from citric acid†

Olivier Bonjour,[a] Ilme Liblikas,[b] Tõnis Pehk,[c] Truong Khai-Nghi,[d] Kari Rissanen,[d] Lauri Vares*[b] and Patric Jannasch*[a,b]

Introducing biobased polymers from renewable sources for use as high-performance thermoplastics with high demands on mechanical rigidity, transparency, thermal stability, as well as good processability, is a significant challenge. In the present work we have designed and prepared a rigid biobased bis-spirocylic diol by di-cycloketalization of a bicyclic diketone (*cis*-bicyclo[3.3.0]octane-3,7-dione, obtained from citric acid) using trimethylolpropane. This spiro-diol monomer has two reactive primary hydroxyl groups and the synthesis from inexpensive biobased starting materials is straightforward and readily upscalable, involving no chromatographic purification. In order to explore the usefulness of the new monomer, it was employed in melt polycondensations with diphenylcarbonate at up to 280 °C to form rigid fully amorphous polycarbonates (**PC**s). Molecular weights (MWs) up to M_n = 28 kg mol^{-1} were achieved, and thermal and dynamic mechanical measurements showed glass transitions up to T_g = 100 °C, with no thermal decomposition until T_d ~350 °C. Solvent cast films had excellent mechanical flexibility and strength, as well as a high transparency with only slight coloration. Results by dynamic melt rheology implied that the high-MW **PC**s had a good processability at 170 °C, with a stable shear modulus over time, but started to degrade *via* chain scission reactions when the temperature approached 200 °C. In conclusion, the present work demonstrates the straightforward preparation of the citric acid-based spiro-diol, and indicates that it is an efficient building block for the preparation of rigid biobased PCs and other condensation polymers.

Received 9th March 2020,
Accepted 27th May 2020

DOI: 10.1039/d0gc00849d

rsc.li/greenchem

Introduction

The development of sustainable biobased alternatives to fossil-based monomers and polymers has become increasingly important in recent years due to growing environmental, social and economic concern.[1,2] However, it is a considerable challenge to chemically design economically viable biobased polymers which meet all the strict requirements from high-end applications on high-performance plastics with good processability.[3] For example, it is crucial that plastics intended for a wide range of automotive, construction, coating and packaging applications have a high degree of transparency and adequate thermal and mechanical properties to maintain dimensions and mechanical strength at elevated temperatures. This requires rigid polymers with a high glass transition temperature (T_g), high molecular weight (MW), as well as high thermal stability. Consequently, there is currently a need for biobased building blocks and monomers containing rigid aromatic and alicyclic rings to produce polymers with inflexible macromolecular chain structures.[3]

Lignin is the most accessible source of rigid aromatic building blocks in the form of various phenolic compounds.[4] However, the depolymerization and purification of lignin is a complex and difficult process and so far vanillin is the only lignin-based compound that is commercially available. Despite these limitations, several high-T_g lignin-based polymers[5] in the form of, *e.g.*, polymethacrylates[6,7] and polyesters,[8–10] have been reported. When it comes to alicyclic monomers for polycondensation processes, isosorbide is probably the most studied and exploited alternative.[11] Isosorbide is a nontoxic and chiral bicylic diol produced from sorbitol, which, in turn,

[a]*Department of Chemistry, Lund University, Box 124, Lund 221 00, Sweden. E-mail: patric.jannasch@chem.lu.se*
[b]*Institute of Technology, University of Tartu, Nooruse 1, Tartu 50411, Estonia. E-mail: lauri.vares@ut.ee*
[c]*Laboratory of Chemical Physics, National Institute of Chemical Physics and Biophysics, Akadeemia tee 23, Tallinn 12618, Estonia*
[d]*University of Jyvaskyla, Department of Chemistry, P.O. Box 35, Survontie 9 B, Jyväskylä 40014, Finland*

†Electronic supplementary information (ESI) available. CCDC 1986990. For ESI and crystallographic data in CIF or other electronic format see DOI: 10.1039/d0gc00849d

is a reduction product of glucose.[12,13] Despite the apparent benefits of incorporating isosorbide into polymers, the limited reactivity and stability are obvious drawbacks.[14] The low reactivity of the two non-equivalent secondary hydroxyl groups[15] impedes the formation of high MW polymers *via* polycondensation, and low MW polymers have insufficient mechanical properties. Increasing the polycondensation temperature (>230 °C) or reaction time to favor polymer chain growth typically leads to discoloration, cross-linking and degradation due to the limited stability towards thermooxidation.[14] Methods to improve the reactivity of isosorbide and other isohexides have been investigated and the strategies include the conversion of the secondary hydroxyl groups into primary ones *via* carbon chain extension,[16,17] and the development of more efficient catalyst systems.[18] Still, the intrinsic instability of the fused furan ring system needs attention. Gao, *et al.* have recently reported on octahydro-2,5-pentalenediol (OPD, Scheme 1), derived from citric acid.[19,20] Just like isosorbide, it has a rigid V-shaped structure, but instead of furan rings it has two *cis*-fused carbocycles. This alicyclic diol yielded PCs with good thermal stability (thermal decomposition at 276 °C) and T_gs up to 80 °C, demonstrating that the mimicking of the isosorbide bicyclic structure is an efficient approach to increase the chain rigidity of polymers. However, similarly to isosorbide, the secondary hydroxyl groups of OPD have low reactivity in polycondensation reactions and are likely to lead to low and medium MW polymers.

The introduction of cyclic ketal and acetal units into polymers is a further attractive strategy to increase the T_g and improve mechanical properties of polymers.[21] When an aldehyde or a ketone reacts with a suitable diol, a cyclic acetal or ketal, respectively, is formed. From this follows that the use of cylic ketones will lead to spiro-cyclic products, which are especially rigid.[21] The reactions proceed *via* acid catalyzed equilibria and the removal of water is necessary to reach high conversion. Acetals and ketals are typically stable towards bases but are susceptible to hydrolysis under acidic conditions.[22] Du Prez and coworkers prepared spirocyclic diol ("spiro-diol") monomers in ketalization reactions of glycerol and two equivalents of 1,4-cyclohexanedione and 4,4′-dicyclohexanone, respectively.[23] Both monomers were successfully used to prepare PCs of high MW, but the synthesis of polyesters proved difficult and only low MW products were obtained. Recently, the biobased diketones camphorquinone and 1,4-cyclohexanedione were combined with glycerol to obtain stiff spiro-diols.[24] The corresponding PCs showed good mechanical properties, high thermal stability and high T_g values. However, the isolation of these diol monomers required chromatographic purification, which makes them less attractive on larger scales. In another piece of work, Mankar *et al.* synthesized a spiro-diol by acetal formation in a reaction of pentaerythritol with two equivalents of vanillin.[25] Incorporation of this rigid spiro-cyclic diol in copolyesters produced from 1,6-hexanediol and dimethyl terephthalate resulted in improved T_g and thermal stability.[25] Hence, this gave materials similar to Akestra™, a commercial fossil-based high-performance polyester produced from a spiro-diol, ethylene glycol and terephthalic acid.[26] Using a similar strategy, Warlin and coworkers reported the synthesis of a rigid spiro-diol from pentaerythritol and two equivalents of fructose-based 5-hydroxymethylfurfural.[27] This monomer was employed to produce polyesters and poly(urethane-urea)s with increased T_gs. However, the investigated spiro-diol was found to be heat-sensitive, causing coloration and branching during the polyester synthesis. Besides the synthesis of various cyclic monomers, polycycloacetals and polycycloketals have been formed

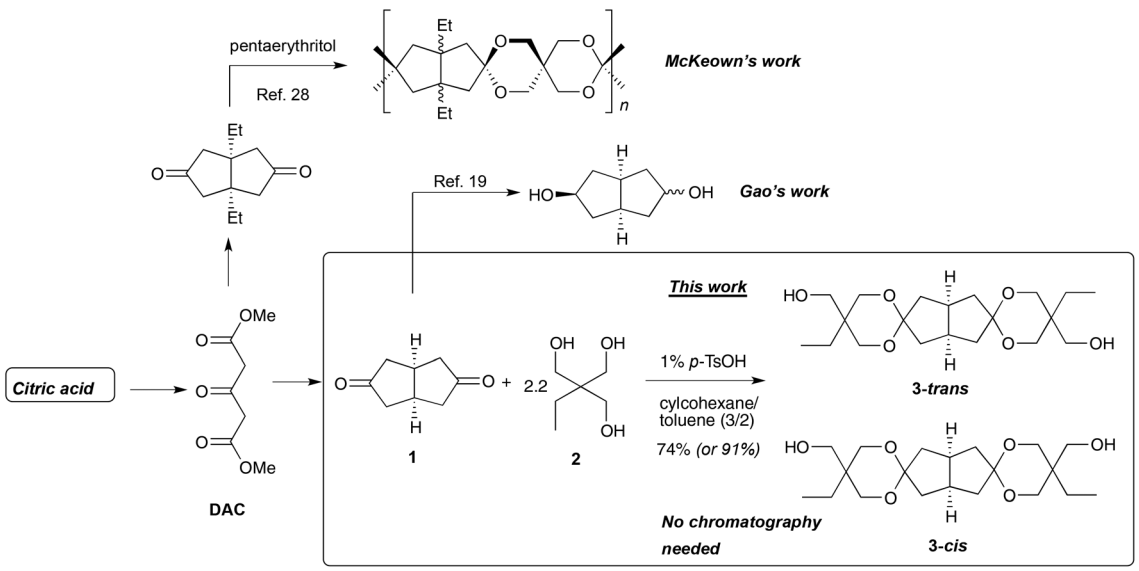

Scheme 1 Outline of the compounds based on diketone **1** reported by McKeown and Gao, and in the present work (inside box). Spiro-diol **3** (mixture of *cis* and *trans*) was synthesized in a ketalization reaction of diketone **1** and a slight excess of TMP **2** (yields of 74 and 91% were obtained when the product was isolated by crystallization and chromatography, respectively).

in direct polycondensations of tetraols and dialdehydes or diketones, respectively.[13] For example, McKeown *et al.* has reacted 1,5-diethylbicyclo[3.3.0]octane-3,7-dione with pentaerythritol in a polycondensation and achieved a spiro-polymer with a very high T_g.[28] However, the degree of polymerization remained mediocre at ~30, and the polymer was rather easily hydrolyzed in solution unless special precautions were taken (Scheme 1).

In the present work we have designed and prepared a novel and readily accessible biobased tetracyclic aliphatic spiro-diol **3** which combines the thermal stability of the rigid V-shaped alicyclic rings with the high reactivity of primary hydroxyl groups installed *via* the spiro rings (Scheme 1). The stiff bicyclic diketone *cis*-bicyclo[3.3.0]octane-3,7-dione **1** was employed as a starting material. This diketone is derived *via* a Weiss–Cook condensation between glyoxal and dimethyl-1,3-acetonedicarboxylate (DAC).[29] Aqueous glyoxal can be prepared *via* oxidation of ethylene glycol.[30] A plant-based ethylene glycol production is currently under development by Avantium N.V.[31] DAC is readily derived from citric acid after decarboxylation and esterification.[32–34] Citric acid is an extensively used biobased platform chemical, produced *via* fermentation of glucose in more than 1.6 million tons annually.[35] Thus, the synthesis route of **1** from citric acid is well-developed and involves only inexpensive acids (cat. H_2SO_4 with H_2O_2 or $ClSO_3H$, aq. HCl, AcOH), base (NaOH) and MeOH. For the ketalization, we employed trimethylolpropane (TMP, **2**), a triol widely used in the polymer industry that is available from Perstorp with partly renewable content (Evyron™).[36] The ketalization reaction between diketone **1** and two equivalents of TMP **2** then afforded the stiff spiro-diol **3**, which bears two six-membered spiro rings connected through a bicyclo[3.3.0] octane entity. Depending on the origin of the TMP (0, 20 or 50% renewable grade), spiro-diol **3** has a 40, 50 or 70% content from renewable sources. Consequently, the overall synthesis route to spiro-diol **3** is well-developed, readily up-scalable, and this monomer can be envisioned as a valuable biobased building block in various applications, including the preparation of different condensation polymers. In order to investigate the usefulness spiro-diol **3**, we have in the present work studied the preparation of PCs in polycondensations with diphenylcarbonate, and subsequently investigated the thermal and mechanical properties, as well as the processability of the resulting materials.

Results and discussion

Monomer synthesis and structure elucidation

A roughly 1 : 1 mixture of two isomers of spiro-diol **3** was formed in the ketalization reaction of diketone **1** with two equivalents of TMP **2** in the presence of an acid catalyst in toluene/cyclohexane (Fig. 1a and Fig. S1–S6†). We speculated that these isomers are diastereomers that differ by mutual orientation of the terminal ethyl and hydroxymethyl groups (Scheme 1). The C_2 symmetric isomer was conveniently named as **3**-*trans* and the C_s symmetric as **3**-*cis*. We separated these two isomers with the aim to unambiguously confirm the diastereomers. This separation turned out to be a routine task by standard flash chromatography on silica gel. The different symmetry of **3**-*trans* and **3**-*cis* is evident from their NMR spectra (Fig. 1 and Table S1†).

In the bicyclo[3.3.0]octane subunit, the *trans* isomer has equivalent C-1 and C-5 and H-1 and H-5 chemical shifts, while the *cis* isomer shows different ones, separated in the ^{13}C and ^{1}H NMR spectra by 2.3 and 0.03 ppm, respectively. Further confirmation of the assignment of stereoisomers was obtained after single crystal X-ray analysis of the *trans* isomer. The single crystals of the compound **3**-*trans* were obtained by slow evaporation of chloroform at ambient temperature. Fig. 2 presents the structure of **3**-*trans*. In the solid-state the ethyl substituents of **3**-*trans* are equatorial, while the hydroxymethyl groups are axial. The crystal lattice is stabilized *via* hydrogen bonds between the hydroxyl groups of **3**-*trans* with its neighboring molecules. Crystal data, data collection and refinement details are given in the ESI.† Despite many attempts, no suitable single crystals from **3**-*cis* could be obtained and thus its X-ray structure could not be determined. In the obtained conformation, the methylene carbons of the dioxane rings have both one *trans* and one *gauche* orientation to the bicycle methylene carbon atoms. However, from two bicycle methylene carbons, only one is having two *gauche* orientations. This is the main reason for the significant differences in the methylene carbon chemical shifts in the bicycle (7.4 in *trans vs.* 6.5 ppm in *cis* isomer) and the quite close values of the methylene carbon chemical shifts from the dioxane rings (for more comprehensive data, see Table S1†).

During the course of the work we optimized the ketalization reaction, work-up and product isolation procedure to increase the efficiency for large scale synthesis of spiro-diol **3**. In a preparative scale we chose to work with the diastereomeric mixture for practical reasons. This is also most relevant from an industrial point of view. We evaluated various solvents (mixtures of cyclohexane/DMF and cyclohexane/toluene, pure toluene), varied the stoichiometry of the reagents (1.95–3.5 eq. of TMP) and the amount of catalyst (1–20 mol% *p*-toluenesulfonic acid, [*p*-TsOH]). The use of toluene as a reaction medium resulted in some darkening during the ketalization, probably due to the relatively high temperature needed for reflux. The lower boiling cyclohexane did not fully dissolve the starting materials. However, the addition of a small amount of DMF (10%) resulted in complete dissolution and a clean reaction. The removal of DMF is nevertheless tedious and its use is not recommended due to toxicity issues.[37] Finally, a 3 : 2 mixture of cyclohexane/toluene was identified as the best solvent system, affording a clean conversion without any noticeable by-product formation. The amount of acid catalyst had only a minor impact on the reaction outcome, and we found 1 mol% of *p*-TsOH to be a suitable concentration. An excess of TMP corresponding to 3.5 equiv. in relation to the diketone resulted in a somewhat faster ketalization reaction. Still, a smaller excess (2.2 equiv., *i.e.* 1.1 equiv. in relation to

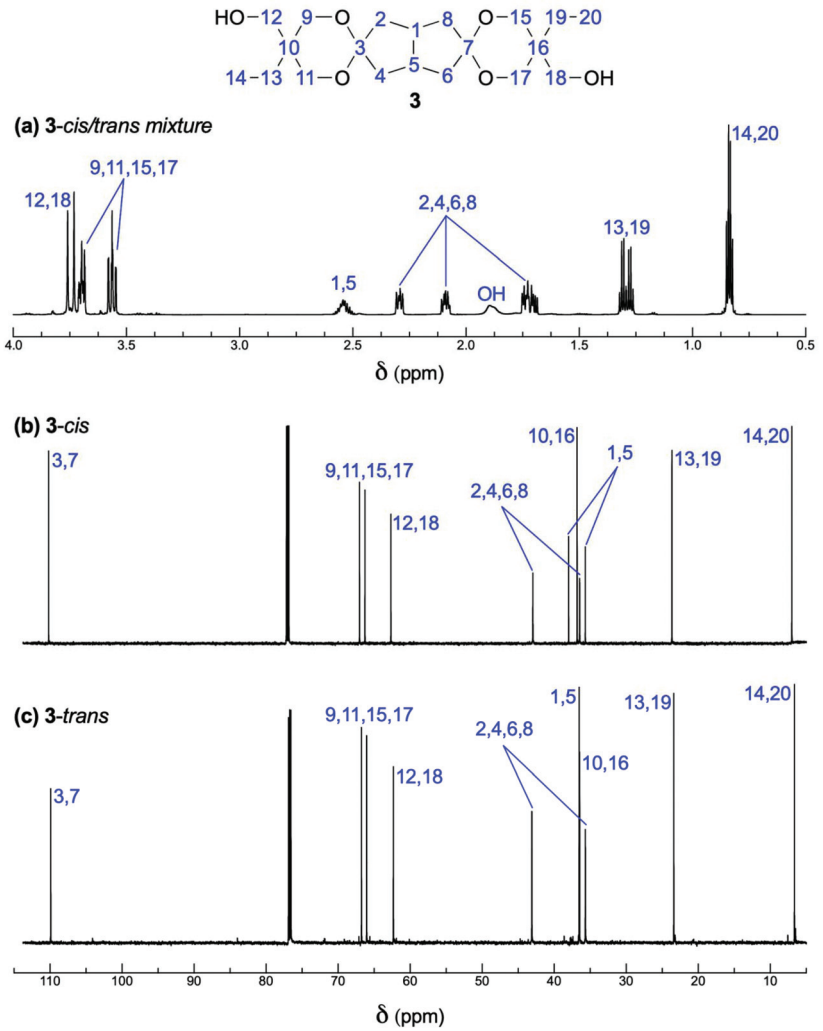

Fig. 1 (a) ^{1}H spectrum of the mixture of **3**-*trans* and **3**-*cis* after isolation *via* double crystallization, and ^{13}C spectra of the (b) **3**-*cis* and (c) **3**-*trans* isomers after separation.

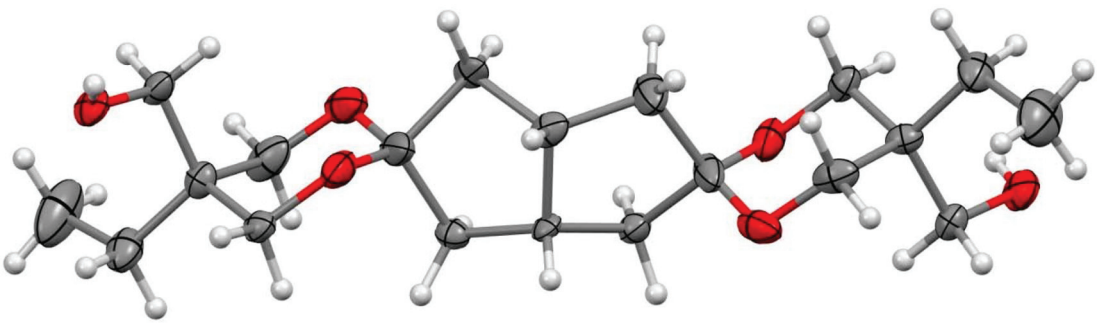

Fig. 2 The X-ray structure of **3**-*trans* (thermal displacement ellipsoids are shown at the 50% probability level).

one carbonyl group) was enough to achieve a high conversion during 16 h. Detailed data from the optimization is presented in Table S2.†

After cooling the reaction mixture and removal of the solvents by evaporation, three different work-up/product isolation methods were evaluated: (a) direct crystallization of **3** in EtOAc/hex, 1 : 1, (b) dissolution of the directly crystallized product in EtOAc, washing with water/brine, followed by a second crystallization, and (c) flash chromatography. The direct crystallization (method a) afforded the crude product in

85% yield. However, by careful analysis of ^{13}C NMR spectra, we detected a small amount of unreacted TMP present in the product. The aqueous wash (method b) removed the traces of TMP and the second crystallization afforded the pure product **3** in 74% yield. Finally, the purification of the crude reaction mixture by flash chromatography (method c) afforded **3** in 91% yield. Still, this method is less attractive from practical and economical points of view.

The hydrolytic stability of spiro-diol **3** in acidic environment was evaluated by using conditions reported by Liu and Thayumanavan[38] after modification: 1% aq. KH_2PO_4 (pH = 4.5) in CD_3CN at 20 and 60 °C, respectively, and 10 mM aq. trifluoroacetic acid (TFA) in CD_3CN at 20 °C. The experiments were carried out directly in NMR tubes and monitored by recording ^1H NMR spectra at regular intervals. In the phosphate buffer at 20 °C, the diol was stable and no degradation was observed even after 7 days. However, after raising to 60 °C traces (<5%) of new signals that correspond to the partially hydrolyzed diol were observed after 24 h. In 10 mM aqueous TFA, the hydrolysis occurred faster. After 4 h at 20 °C roughly 50% of spiro-diol **3** was left, and after 24 h all the diol had been cleanly converted into diketone **1** and TMP **2** (see Fig. S11† for ^1H NMR spectra at different time intervals).

Polycarbonate preparation and structure characterization

The diastereomeric mixture of spiro-diol **3** was employed in the synthesis of PCs using diphenylcarbonate (DPC) as the carbonyl source (Scheme 2). Polymerizations were carried out as solvent-free melt polycondensations and we initially evaluated two different catalysts [$NaHCO_3$, Li(Acac)], varied the ratio **3** : DPC, and experimented with various heating/vacuum profiles (see Table S3† for detailed descriptions). A procedure adapted from Du Prez *et al.* was used as a starting point.[23] After this optimization to control MW and avoid degraded products, we prepared two **PC** samples using $NaHCO_3$ as catalyst and keeping the molar ratio of diol **3** and DPC at 1.0 : 1.1. The MW of the first sample was purposely kept low and the second one high, to give the samples denoted **PC**-*l* and **PC**-*h*, respectively (Scheme 2). In the preparation of **PC**-*h*, melt polycondensation temperatures up to 280 °C were applied, whereas for **PC**-*l* the maximum temperature was limited to 210 °C. In the final stage when the temperature was raised to 280 °C, **PC**-*h* became highly viscous and started slowly to darken, after which the polymerization was terminated. In contrast, **PC**-*l* remained a viscous flowing melt throughout the polycondensation at 210 °C with no apparent color change. Both **PC**-*l* and **PC**-*h* were purified by precipitation in methanol from chloroform solutions. Further details on their synthesis are given in the Experimental section.

Characterization by size-exclusion chromatography (SEC) using poly(ethylene oxide) standards showed M_n = 7.5 and 27.7 kg mol^{-1} for **PC**-*l* and **PC**-*h*, respectively (Table 1). As anticipated, **PC**-*h* reached a high MW, while that of **PC**-*l* was significantly lower. Moreover, the analysis revealed polydispersities of $Đ$ = 3.55 and 3.40, respectively. Under normal (ideal) conditions a value of $Đ$ close to 2 is expected for polycondensations driven to high monomer conversions.[39] Hence, the higher values obtained in the present case may imply limited degradation *via* ring opening of the ketal rings during the polymerizations, which would result in branching and a broadening of the chain length distribution. This was also hinted by the shape of the SEC curves, which show high-MW shoulders (Fig. S12†). Similar findings have previously been reported by Du Prez *et al.* who found $Đ$ in the range 2.8–3.2 for **PC**s (M_n = 24–33 kg mol^{-1}) prepared by melt polycondensation of DPC and ketal diol monomers.[23] For polyesters based on the same ketal monomers, the range in $Đ$ was 2.3–4.0. In addition, Suh and coworkers synthesized a **PC** by polycondensation of DPC and the bis(glycerol) ketal of camphorquinone, and reported $Đ$ = 2.25 (M_n = 8.3 kg mol^{-1}).[24]

Characterization by ^1H and ^{13}C NMR spectroscopy confirmed the structure of the **PC**s (see Fig. 3 and Fig. S7 and S8†). Detailed analysis of the spectra of **PC**-*h* indicated that the *cis* and *trans* isomers of **3** preserved the shift differences. The carbonyl region at 155 ppm revealed the dyad level sequences of the polymer, showing clearly the presence of *cis–cis*,

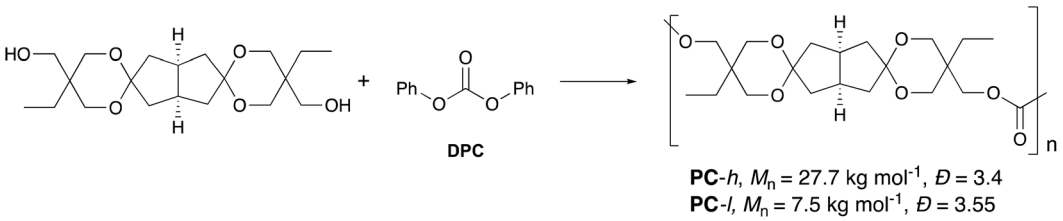

Scheme 2 Synthesis of PCs by melt polycondensations of diol **3** with DPC using the mixture of the **3**-*trans* and **3**-*cis* isomers.

Table 1 Data on the **PC**s based on diol **3**

Sample	Isolated yield (%)	M_n (SEC) (kg mol^{-1})	$Đ$ (SEC)	M_n (NMR) (kg mol^{-1})	T_g (DSC) (°C)	T_g (DMA) (°C)	$T_{d,95}$ (TGA) (°C)
PC-*l*	86	7.5	3.55	7	85	85	352
PC-*h*	90	27.7	3.40	22	100	99	360

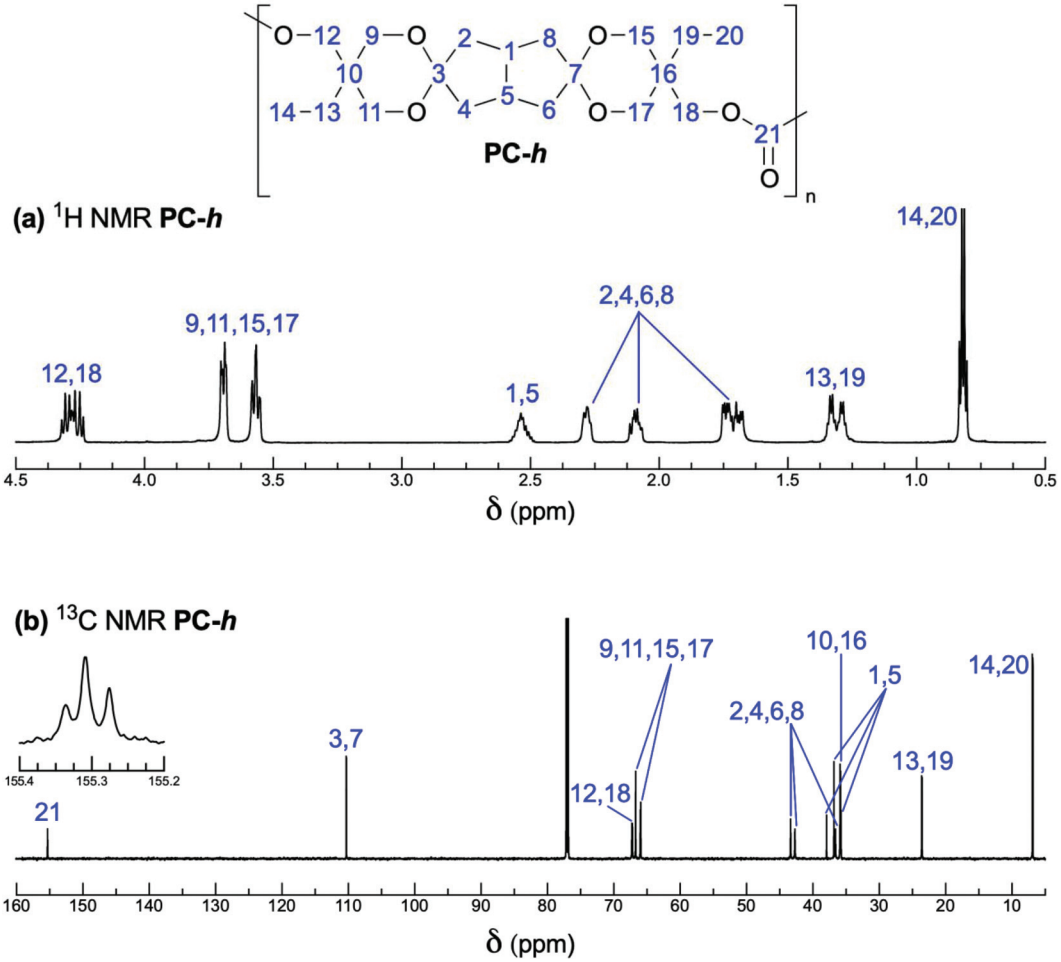

Fig. 3 (a) ^{1}H and (b) ^{13}C spectra of **PC**-*h*. ^{13}C signals indicating the 1 : 2 : 1 ratios of *cis–cis*, *cis–trans* and *trans–trans* dyads are shown separately in the carbonyl region.

cis–trans and *trans–trans* dyads in roughly 1 : 2 : 1 ratios (Fig. 3). This indicates that the reactivity of each hydroxyl group is independent, and is hence not influenced by the relative orientation of the other hydroxyl group in diol **3**. Close inspection of the ^{1}H and ^{13}C NMR spectra also indicated the complete lack of any aromatic signals potentially originating from DPC residues at the chain ends. On the other hand, small signals from terminal –*C*H$_2$OH groups were clearly present at 62.7 ppm in the ^{13}C NMR spectra (Fig. S9 and S10†). Assuming linear chains with exclusively –*C*H$_2$OH end groups, the intensity of these signals in the spectra of both **PC**-*l* and **PC**-*h* were in level with that expected from their respective degree of polymerization measured by SEC. Hence, the end group analysis based on the signals from terminal –*C*H$_2$OH groups indicated M_n = 7.0 and 22 kg mol^{-1} for **PC**-*l* and **PC**-*h*, respectively. The slightly lower values obtained in the end group analysis may indicate limited branching, which is in agreement with the finding that $Đ > 2$. Still, we cannot rule out that the observed differences in the M_n values are explained simply because SEC analysis using poly(ethylene oxide) standards and calculations based on small NMR signals give different results.

After drying, the precipitates of both **PC**-*l* and **PC**-*h* were completely soluble in $CHCl_3$ and THF, partially soluble in 1,4-dioxane, EtOAc and toluene, and insoluble in water, MeOH, iPrOH, acetone, hexanes, diethyl ether and CH_3CN. The **PC**-*h* precipitate had a "cotton-like" appearance with clearly visible fibers, reflecting its high MW, while the **PC**-*l* precipitate was a fine powder as expected from its low MW. Both **PC** samples were cast from solution to study their ability to form films. The **PC**-*h* films were only slightly colored (Fig. 4) with high transparency (Fig. S13†) and gloss (between 75 and 118 gloss units [GU]), combined with an excellent mechanical flexibility (ESI Movie†) and strength (Fig. S14†). The films formed by **PC**-*l* were less colored, equally transparent, but showed brittleness due to the lower MW.

Thermal characterization

The T_g and the thermal decomposition temperature ($T_{d,95}$) of the **PC**s were evaluated by DSC and TGA measurements, respectively. At the T_g the polymer starts to soften and lose its mechanical rigidity, and hence this value normally sets the upper use temperature in a given application. As seen in

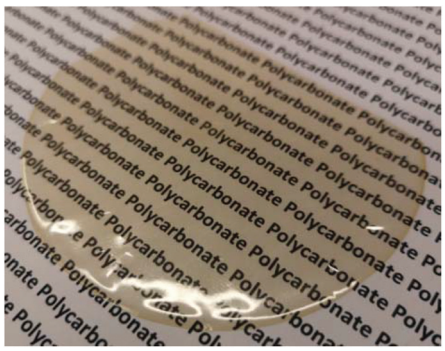

Fig. 4 Photograph of a 45 μm thick film of **PC**-*h* cast from $CHCl_3$ solution.

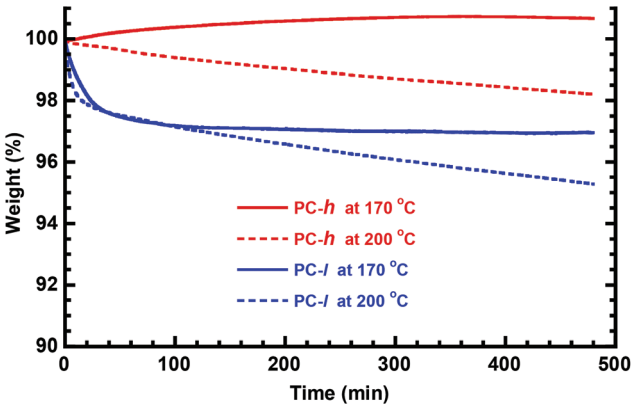

Fig. 6 Isothermal TGA measurements of **PC**-*l* and -*h* at 170 and 200 °C.

Fig. 5a, **PC**-*h* showed T_g = 100 °C, which is in range with polystyrene.[40] As expected, the DSC traces did not show any crystallization or melt transitions. Hence, **PC**-*h* is a fully amorphous polymer that will retain mechanical rigidity at temperatures approaching 100 °C. Poly(trimethylene carbonate) and poly(propylene carbonate) have T_g values at approximately −17 °C[41] and 30 °C,[42] respectively, which demonstrates that the incorporation of the tetracyclic spiro-diol **3** has the potential to significantly increase the T_g of aliphatic PCs. The high T_g of **PC**-*h* may open up for, *e.g.*, "hot-fill" applications in food packaging and handling. The value may further be compared to the semicrystalline PET (T_g = 75 °C),[43] as well as with PC based on bisphenol A (T_g ~150 °C),[44] and the Akestra™ family of polyesters (T_g in the range 90–110 °C, depending on monomer content).[26] The DSC analysis of **PC**-*l* showed a T_g value of 85 °C, *i.e.*, 15 °C below that of **PC**-*h*. This was anticipated because of the significantly lower M_n value of the former polymer (7.5 *vs.* 27.7 kg mol^{-1}). The lower T_g and M_w values suggest potential applications as, *e.g.*, specialty polyols in the preparation of polyurethanes.

The $T_{d,95}$ value measured by TGA analysis typically determines the maximum melt processing temperature of a polymer. Both **PC**-*h* and -*l* show thermal decomposition in a single step at $T_{d,95}$ ~350 °C (Fig. 5b). This indicated that the thermal stability of these materials is sufficiently high to allow melt processing which (depending on method, MW, *etc.*) is typically performed *ca.* 50–100 °C above T_g. In order to study the long-term stability, isothermal TGA measurements were carried out at 170 and 200 °C, respectively, during 8 h with the samples in the melt state. As seen in Fig. 6, the two **PC** samples showed different behavior under these conditions. At 170 °C, **PC**-*l* showed an initial weight loss of just above 2 wt%, before reaching a plateau. At 200 °C the initial weight loss had the same magnitude, but was followed by a constant weight loss (decomposition) rate of ~0.30 wt% per h. The initial weight loss may be due to the presence residual solvent or monomer. For **PC**-*h*, the weight slowly increased by ~0.8 wt% and then seemed to reach a plateau value. This increase was most probably due to limited oxidation of the sample. In contrast, the same sample displayed a steady weight loss rate of ~0.15 wt% per h at 200 °C, *i.e.*, half that of **PC**-*l*.

Dynamic mechanical characterization

The dynamic mechanical properties of the **PC**s were studied by DMA analysis of hot-pressed sample bars at 1 Hz in the linear viscoelastic region (tensile strain 0.02%). Fig. 7 shows the tensile storage (E') and loss (E'') moduli of the two **PC** samples during heating at a rate of 2 °C min^{-1}. As can be seen, the E' value on the glassy plateau was higher for **PC**-*h* because of its higher M_n value compared to **PC**-*l*. Consequently, **PC**-*h* had an

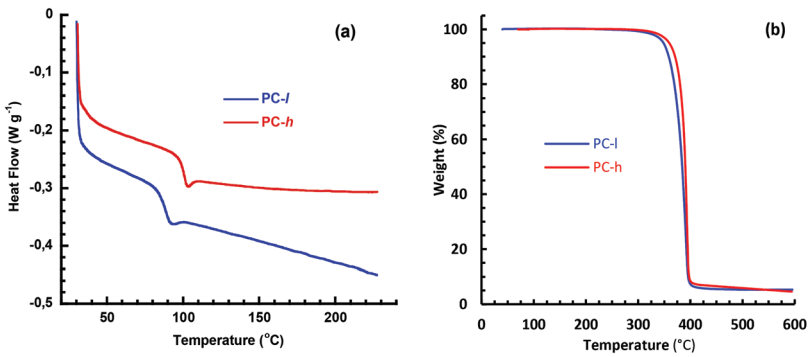

Fig. 5 DSC (a) and TGA (b) traces of **PC**-*h* and -*l*, respectively.

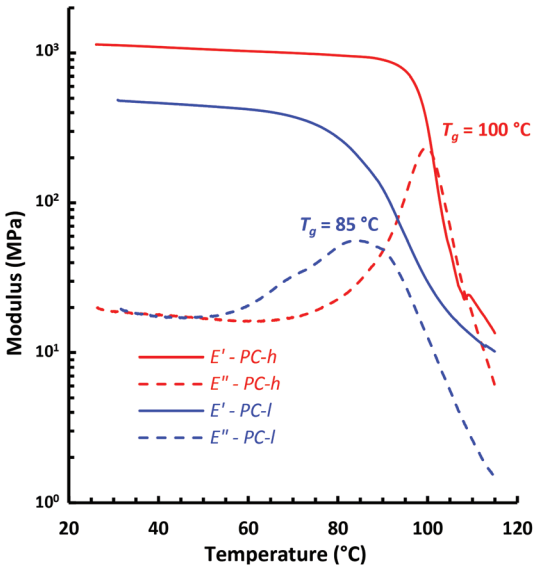

Fig. 7 Tensile storage (E') and loss (E'') moduli of **PC**-*l* and -*h*, as measured by DMA at 1 Hz, 0.02% strain.

E' value of 0.90 GPa at 90 °C, while **PC**-*l* had an E' value of 0.42 GPa at 60 °C. The decrease in E' marked the start of the glass transitions of the two **PC**s. Notably, the transition occurred in a broader temperature range for **PC**-*l* than for **PC**-*h*, which may be a consequence of the broader $Đ$ value and hence larger heterogeneity of the former sample. After the transition region, *i.e.*, just before entering the rubbery plateau, the samples deformed too much to continue the measurements. The T_g was indicated by the maximum in E'' and showed T_g = 85 and 100 °C for **PC**-*l* and **PC**-*h*, respectively. These values were essentially the same as those evaluated by DSC, which demonstrated a very good correlation between the two methods.

Dynamic melt rheology

Dynamic rheology measurements were primarily carried out to assess the stability and processability of the **PC**s in the melt state. Rheological properties are related to MW and structure, and changes in the modulus may thus indicate degradation by, *e.g.*, polymer chain scission or crosslinking reactions.[45] The data of the present polymers was measured by using hot-pressed sample discs in a parallel plate arrangement. Time sweeps were carried out during 20 min at a frequency of 1 Hz at 0.2% strain, which was within the linear viscoelastic region.

Fig. 8a shows the melt shear storage modulus (G') and phase shift (δ) of **PC**-*h* as a function of time at 170 and 200 °C, respectively. As can be seen, the data at 170 °C were constant over time with G' and δ equal to 42 kPa and 43°, respectively. This indicated a high stability of the sample without apparent signs of any polymer chain degradation. Initially, the measurement at 200 °C showed a decrease in G' and an increase in δ, in relation to the data at 170 °C. This was consistent with the expected decrease in viscosity and less elastic response of the melt as $T - T_g$ increased. In sharp contrast to the data at 170 °C, there was a clear decrease in G' and a corresponding increase in δ observed over time at 200 °C. These changes towards a less elastic material are consistent with a reduction in MW over time. Hence, the data in Fig. 8a implies that **PC**-*h* is processable in the melt at 170 °C, but starts to degrade by chain scission reactions when the temperature approaches 200 °C.

Fig. 8b shows the corresponding values of G' and δ of **PC**-*l* as a function of time at 170 °C. Compared to the data of **PC**-*h*, the initially measured value of G' was lower and the δ value higher. This was consistent with the lower MW of **PC**-*l*, resulting in a less elastic response. Over time, the data of **PC**-*l* showed a clear increase in G' and a corresponding decrease in δ. These trends towards a more elastic material are consist-

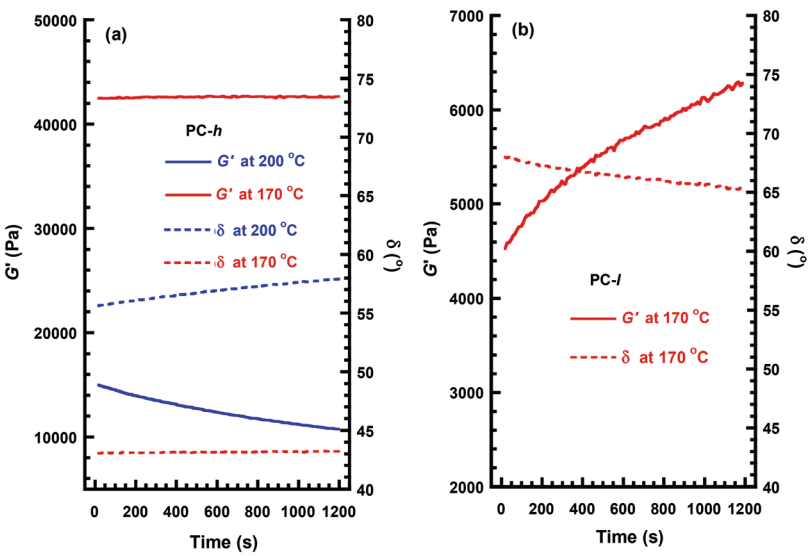

Fig. 8 Variation of the melt shear storage modulus (G') and phase shift (δ) during time sweeps of **PC**-*h* at 170 and 200 °C (a) and **PC**-*l* at 170 °C (b), as measured by rheology at 1 Hz, 0.2% strain (note the different scales for G').

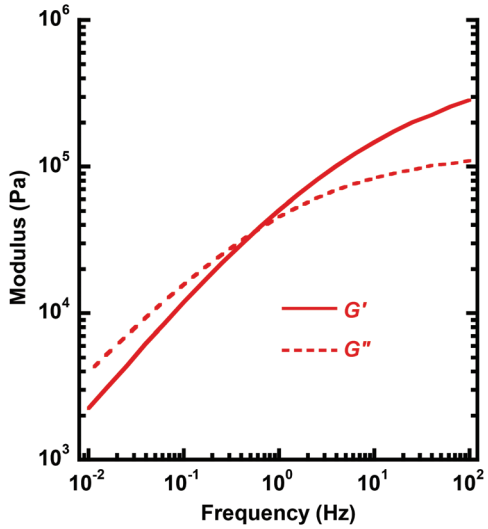

Fig. 9 Melt shear storage (G') and loss (G'') modulus of **PC**-*h* as a function of frequency at 170 °C (0.2% strain).

ent with the occurrence of crosslinking reactions. In conclusion, chain scission dominated the degradation of the high-MW **PC**-*h* at high temperature, while the lower MW **PC**-*l* (with a higher concentration of chain ends) instead degraded by crosslinking. However, at 170 °C the **PC**-*h* melt showed a very stable rheological behavior without any signs of degradation. This temperature was 70 °C above the T_g and 180 °C below the $T_{d,95}$, which indicates a good processability of **PC**-*h*. Fig. 9 shows a frequency sweep in the range 0.01–100 Hz on **PC**-*h* at 170 °C. At low frequency, the shear loss modulus (G'') dominated in the viscous melt region. However, at approx. 0.6 Hz there was a crossover, and G' instead started to dominate as the sample approached the rubbery plateau.

Hydrolytic stability study

The current **PC**s contain potentially sensitive ketal groups which motivated a preliminary investigation of the hydrolytic stability. Ketal groups are typically quite stable under basic conditions but tend to degrade at low pH.[22] Sample pieces of **PC**-*h* were immersed in aqueous solutions with pH = 3 and pH = 8, respectively, at 37 °C during 18 days. After the immersion, the samples were dried, weighed, and analyzed by SEC to evaluate any decrease in MW. However, no changes in sample weight, M_n or $Đ$ were detected. Consequently, the ketal-containing **PC**-*h* was seemingly stable under these conditions, at least partly because of its high T_g. The susceptibility of ketal and acetal groups in polymers to hydrolyze varies and depends on the precise molecular structure.[22]

Experimental section

Materials

All reagents and solvents were obtained from commercial sources and used without further purification. Diketone **1** was synthesized from commercial DAC (purity 97%) according to the published procedure.[46] TMP and DPC were obtained from Acros and had 98% and 99% purity grades, respectively. Reactions were monitored by thin-layer chromatography (TLC, Alugram Xtra SIL G/UV_{254}), and TLC plates were visualized by staining with vanilla or phosphomolybdic acid solution. Silica gel 60 (0.040–0.063 mm, 230–400 mesh) was used in the flash chromatography.

Synthesis of spiro-diol 3

A stirred mixture of bicyclo[3.3.0]octane-3,7-dione **1** (5.39 g, 39.1 mmol), trimethylolpropane (11.53 g, 85.9 mmol, 2.2 eq.), *p*-toluenesulfonic acid monohydrate (74 mg, 0.39 mmol), toluene (50 mL), and cyclohexane (75 mL) was refluxed for 16 h in a 250 mL round-bottom flask equipped with a Dean-Stark water trap. After cooling the reaction mixture to room temperature, the solvent was removed using a rotary evaporator. The crude product was then crystallized from the mixture of EtOAc and hexane to yield 12.26 g (85%) of diol **3** containing some unreacted TMP. This sample was dissolved in EtOAc (200 mL), washed with water (2 × 50 mL) and brine (30 mL), dried over $MgSO_4$, filtered, and concentrated under reduced pressure. The second crystallization yielded 10.64 g (74%) of spirodiol **3** as a white crystalline compound.

Following an alternative procedure, diol **3** was isolated by chromatography. A stirred mixture of bicyclo[3.3.0]octane-3,7-dione **1** (3.70 g, 26.8 mmol), TMP (12.57 g, 93.8 mmol, 3.5 eq.), *p*-toluenesulfonic acid monohydrate (0.05 g), DMF (15 mL), and cyclohexane (110 mL) was refluxed for 8 h in a 250 mL round-bottom flask equipped with a Dean-Stark water trap. After cooling the reaction mixture to room temperature, $NaHCO_3$ (1.0 g) was added and the solvent was removed by using a rotary evaporator. Next, toluene (100 mL) was added and the solid material was filtered off. The mixture was concentrated once more to remove DMF together with toluene. The residue was dissolved in small amount of DCM before loading on the top of the flash chromatography column. A gradual elution system (20–100% EtOAc in petrol ether) was used to afford 9.05 g (91%) of diol **3** (fractions of **3**-*trans* and **3**-*cis* were combined). The same elution system was used to separate the isomers. **3**-*Trans* eluted faster [R_f = 0.56 (70% EtOAc in petrol ether)] than **3**-*cis* [R_f = 0.39 (70% EtOAc in petrol ether)]. The assigned NMR data on the **3**-*trans* and **3**-*cis* isomers is presented in Table S1.†

For the HRMS, IR and Mp measurements, a mixture of *cis* and *trans* isomers were used.

HRMS (ESI): calcd for $C_{20}H_{34}O_6$ $[M + Na]^+$ 393.2248, found 393.2249.

IR (ATR) ν_{max} (cm^{-1}): 3433, 2966, 2862, 1471, 1313, 1134, 1112, 1043, 879, 758.

Mp = 102–103 °C.

Polycondensations

The PCs were synthesized by melt polycondensations using a Büchi Kugelrohr device with Glass Oven B-585 using a round-bottom tube (25 × 140 mm) as a reaction vessel. Representative

procedures for the preparation of **PC**-*h* and **PC**-*l* are given below.

PC-*h*: Spiro-diol **3** (2.017 g, 5.44 mmol), diphenylcarbonate (1.283 g, 5.99 mmol, 1.1 eq.) and $NaHCO_3$ (11 mg, 0.6 mol%) were weighed and placed in the reaction tube. The reaction tube was placed into the Büchi apparatus and the mixture was melted at 115 °C at a rotation rate of 30 rpm. Subsequently the flask was degassed under vacuum (100 mbar) and purged with argon three times before heating the reaction mixture. First, the tube was kept at 160 °C for 1.5 h at atmospheric pressure followed by 20 min at 200 mbar. Then the temperature was increased at constant speed to 200 °C during 1.5 h and kept for 45 min. Next, the pressure was reduced to 100 mbar and after 30 min the temperature was increased to 220 °C. During the next 2 h, the temperature was gradually increased to 260 °C, and the pressure reduced to 0.36 mbar. The rotation rate of the reaction vessel was reduced to 6 rpm as the reaction mixture became very viscous. In the final stage, the temperature was raised to 280 °C during 1 h. The product was then cooled down to room temperature, dissolved in chloroform (30 mL), and precipitated in ice cold methanol (350 mL). Finally, the precipitate was filtered and dried under vacuum during 40 h to afford 1.944 g of **PC**-*h*. The assigned NMR data of **PC**-*h* is presented in Table S1.†

PC-*l*: Spiro-diol **3** (2.205 g, 5.95 mmol), diphenylcarbonate (1.402 g, 6.55 mmol, 1.1 eq.) and $NaHCO_3$ (8 mg) were weighed into the reaction vessel and placed into a Büchi oven. The reaction mixture was melted, degassed and kept under a blanket of argon at 120 °C. After that the reaction mixture was heated to 160 °C and kept for 2 h. During the second hour at 160 °C, moderate vacuum (50 mbar) was applied. Next, the temperature was gradually raised to 200 °C over 30 min while keeping the vacuum constant (50 mbar). Over the next hour, the temperature was increased to 210 °C and the pressure was gradually reduced to 0.3 mbar. After 15 min under these conditions (210 °C, 0.3 mbar), the reaction mixture was cooled, dissolved in chloroform (30 mL), whereafter the product was precipitated in cold methanol (350 mL). After filtration and drying 2.05 g of **PC**-*l* was obtained.

Structural characterization

The structure of monomers and polymers was determined by NMR spectroscopy using a Bruker 800 or 400 MHz spectrometer with the samples dissolved in chloroform-*d*. The ^1H NMR and ^{13}C NMR spectra were recorded at 800 or 400 MHz and 201 or 101 MHz, respectively. The chemical shifts were calibrated using residual solvent signals (for ^1H, $CDCl_3$: δ = 7.26 ppm, for ^{13}C, $CDCl_3$: δ = 77.0 ppm) and are given in ppm. The HRMS analysis of **3** was performed using a Thermo Electron LTQ Orbitrap XL analyzer and FTIR was recorded using Shimadzu IRAffinity-1 spectrophotometer. The MWs of the **PC**s were determined by size-exclusion chromatography (SEC) in $CHCl_3$. The SEC setup included three Shodex columns coupled in series (KF-805, -804, and -802.5) placed in a Shimadzu CTO-20A prominence column oven, a Shimadzu RID-20A refractive index detector, with Shimadzu LabSolution software. All samples were run at 40 °C at an elution rate of 1 mL min^{-1}. Calibration was done by using poly(ethylene oxide) standards (M_n = 3.86, 12.60, 49.64 and 96.1 kg mol^{-1}).

Thermogravimetry and calorimetry

Thermogravimetric analysis (TGA) was performed on a TA Instruments TGA Q500. Samples of 1–5 mg were heated to 600 °C at a rate of 10 °C min^{-1} under nitrogen flux (60 mL min^{-1}). The thermal decomposition temperature ($T_{d,95}$) was determined at 5% loss of the total weight.

Differential scanning calorimetry (DSC) measurements were performed on TA Instruments DSC Q2000. Samples from 2–7 mg were first heated up to 150–250 °C (depending on their respective thermal decomposition temperature) at a rate of 10 °C min^{-1}. They were kept at this temperature for 2 min, then cooled to −50 °C and kept isothermal for 2 min before being heated up again to the previous temperature, at the same heating rate.

Dynamic mechanical measurements

Dynamic mechanical analysis (DMA) was carried out on TA Instruments DMA Q800. Rectangular bars of **PC**-*h* and **PC**-*l* (dimensions: 35 × 5 × 1 mm^3) were hot-pressed between two Teflon plates using a hydraulic press (Specac, GS15011) at 150 °C during 2 min, then cooled to 100 °C during 5 min, and finally cooled to room temperature. The samples were analyzed at a frequency of 1 Hz, over the temperature range between 25 to 150 °C at a heating rate of 2 °C min^{-1}. The measurements were carried out in the linear viscoelastic region at a strain of 0.02%. The T_g value was determined at the maximum peak value of the loss modulus.

Melt rheology

Dynamic rheology measurements were performed with TA Instruments Advanced Rheometer AR2000 ETC. The experiments were made using parallel plates (∅ = 25 mm). Discs of **PC**-*h* and **PC**-*l* (∅ = 25 mm, t = 1 mm) were hot-pressed as described above. A time sweep was carried out during 20 min at 170 and 200 °C, at a frequency of 1 Hz at 0.2% strain, which was within the linear viscoelastic region. Moreover, a frequency sweep was performed on **PC**-*h* at 170 °C, under a strain of 0.2% over the range 0.01–100 Hz.

Measurements of optical transmission and gloss

Polymer optical transmission measurements were performed on a Perkin Elmer Lambda 40 UV/VIS Specrometer using 32 μm thick film of **PC**-*h* cast from $CHCl_3$ solution. The gloss was measured using a Byk Gardner Spectro-guide at 60° angle. Two **PC**-*h* films of different thicknesses (cast from $CHCl_3$) were used and the measurements were repeated three times.

Conclusions

We have successfully developed a straightforward and readily upscalable synthetic pathway to a biobased alicyclic monomer

using inexpensive starting materials. Hence, a bicyclic ketone derived from citric acid was reacted with two equivalents of trimethylolpropane in a ketalization reaction to form the spirocyclic diol in high yields. This product carried two primary hydroxyl groups and was obtained as an equimolar mixture of *cis* and *trans* isomers. In an initial evaluation of this spiro-diol, we developed and carried out melt polycondensations of the new monomer and diphenylcarbonate to produce rigid PCs. The results showed that products with high MWs and T_g values up to 100 °C were achieved. Still, further analysis indicated that the products were slightly branched. This hinted that a limited ring opening of the ketal units occurred during the polycondensations, which were carried out at temperatures up to 280 °C. After hot-pressing and solvent casting, the PC formed flexible and mechanically strong samples with high transparency and only slight coloration. Melt rheology implied that the polymer had good processability up to at least 170 °C, but started to degrade as the temperature approached 200 °C. Overall, the results indicate that the citric acid-based spiro-diol is an efficient building block for the preparation of high-T_g condensation polymers. We are currently investigating the use of the spiro-diol monomer to prepare polyesters, polyurethanes and polyacrylates.

Conflicts of interest

There are no conflicts to declare.

Acknowledgements

This work was supported by the European Regional Development Fund (project no. MOBTT21) and the Estonia-Russia Cross Border Cooperation Programme (ER30). O. B. is grateful to the Swedish Research Council Formas for financial support (diarienr 2016-00468), and P. J. acknowledges funding by the Swedish Foundation for Strategic Environmental Research through the "STEPS" project (no. 2016/1489). T. P. thanks The Estonian Ministry of Education and Research (grant no. IUT23-7) and the European Regional Development Fund (grant no. TK134). We are grateful to Jevgenija Martõnova and Prof. Riina Aav for obtaining single crystals for X-ray and this was supported by the Estonian Research Council (grant PRG339). Dr Janek Peterson (Akzo Nobel Baltics) is acknowledged for the gloss measurements. Sergo Kasvandik and Merilin Saarma are thanked for HRMS analyses, Dr Koit Herodses for the UV/Vis measurements and Livia Matt for preparing the SEC and NMR graphs.

References

1 D. K. Schneiderman and M. A. Hillmyer, *Macromolecules*, 2017, **50**, 3733–3749.
2 J. S. Luterbacher, D. Martin Alonso and J. A. Dumesic, *Green Chem.*, 2014, **16**, 4816–4838.
3 H. T. H. Nguyen, P. Qi, M. Rostagno, A. Feteha and S. A. Miller, *J. Mater. Chem. A*, 2018, **6**, 9298–9331.
4 Z. Sun, B. Fridrich, A. de Santi, S. Elangovan and K. Barta, *Chem. Rev.*, 2018, **118**, 614–678.
5 B. M. Upton and A. M. Kasko, *Chem. Rev.*, 2016, **116**(4), 2275–2306.
6 A. L. Holmberg, K. H. Reno, N. A. Nguyen, R. P. Wool and T. H. Epps III, *ACS Macro Lett.*, 2016, **5**(5), 574–578.
7 A. L. Holmberg, N. A. Nguyen, M. G. Karavolias, K. H. Reno, R. P. Wool and T. H. Epps III, *Macromolecules*, 2016, **49**(4), 1286–1295.
8 L. Mialon, A. G. Pemba and S. A. Miller, *Green Chem.*, 2010, **12**, 1704–1706.
9 J. Zhang, C. C. Pang and G. L. Wu, *RSC Adv.*, 2016, **6**, 11848.
10 A. Llevot, E. Grau, S. Carlotti, S. Grelier and H. Cramail, *Polym. Chem.*, 2015, **6**, 6058–6066.
11 D. J. Saxon, A. M. Luke, H. Sajjad, W. B. Tolman and T. M. Reineke, *Prog. Polym. Sci.*, 2020, **101**, 101196.
12 C. Dussenne, T. Delaunay, V. Wiatz, H. Wyart, I. Suisse and M. Sauthier, *Green Chem.*, 2017, **19**, 5332–5344.
13 F. Delbecq, M. R. Khodadadi, D. Rodriguez Padron, R. Varma and C. Len, *Mol. Catal.*, 2020, **482**, 110648.
14 F. Fenouillot, A. Rousseau, G. Colomines, R. Saint-Loup and J. P. Pascault, *Prog. Polym. Sci.*, 2010, **35**, 578–622.
15 B. A. J. Noordover, V. G. van Staalduinen, R. Duchateau, C. E. Koning, B. van, M. Mak, A. Heise, A. E. Frissen and J. van Haveren, *Biomacromolecules*, 2006, **7**, 3406–3416.
16 J. Wu, S. Thiyagarajan, C. Fonseca Guerra, P. Eduard, M. Lutz, B. A. J. Noordover, C. E. Koning and D. S. van Es, *ChemSusChem*, 2017, **10**, 3202–3211.
17 P. Villo, L. Matt, L. Toom, I. Liblikas, T. Pehk and L. Vares, *J. Org. Chem.*, 2016, **81**, 7510–7517.
18 W. Qian, X. Tan, Q. Su, W. Cheng, F. Xu, L. Dong and S. Zhang, *ChemSusChem*, 2019, **12**, 1169–1178.
19 X. Liu, C. Pang, J. Ma and H. Gao, *Macromolecules*, 2017, **50**, 7949–7958.
20 C. Pang, X. Jiang, Y. Yu, X. Liu, J. Lian, J. Ma and H. Gao, *ACS Sustainable Chem. Eng.*, 2018, **6**, 17059–17067.
21 A. Hufendiek, S. Lingier and F. E. Du Prez, *Polym. Chem.*, 2019, **10**, 9–33.
22 E. H. Cordes and H. G. Bull, *Chem. Rev.*, 1974, **74**, 581–603.
23 S. Lingier, Y. Spiesschaert, B. Dhanis, S. De Wildeman and F. E. Du Prez, *Macromolecules*, 2017, **50**, 5346–5352.
24 G.-H. Choi, D. Y. Hwang and D. H. Suh, *Macromolecules*, 2015, **48**, 6839–6845.
25 S. V. Mankar, M. N. Garcia Gonzalez, N. Warlin, N. G. Valsange, N. Rehnberg, S. Lundmark, P. Jannasch and B. Zhang, *ACS Sustainable Chem. Eng.*, 2019, **7**, 19090–19103.
26 Akestra™ by Perstorp AB, CAS number: 102070-64-4, https://www.perstorp.com/en/products/akestra_100.
27 N. Warlin, M. N. Garcia Gonzalez, S. Mankar, N. G. Valsange, M. Sayed, S.-H. Pyo, N. Rehnberg, S. Lundmark, R. Hatti-Kaul, P. Jannasch and B. Zhang, *Green Chem.*, 2019, **21**, 6667–6684.

28 S. Makhseed and N. B. McKeown, *Chem. Commun.*, 1999, 255–256.
29 S. H. Bertz, J. M. Cook, A. Gawish and U. Weiss, *Org. Synth.*, 1986, **64**, 27–38.
30 G. Mattioda and A. Blanc, *Ullmann's Encyclopedia of Industrial Chemistry*, 2011, DOI: 10.1002/14356007.a12_491.pub2.
31 https://www.avantium.com/technologies/ray/.
32 R. Adams, H. M. Chiles and C. F. Rassweiler, *Org. Synth.*, 1925, **5**, 5.
33 E. Jakfalvi, B. L. Gregorne, T. Morasz, G. Toth, A. Szabo, J. Toereki and S. Olah, WO2004089867A2, 2004.
34 Y. Chen, J. Chen and L. Heng, CN103288629A, 2013.
35 C. R. Soccol, L. P. S. Vandenberghe, C. Rodrigues and A. Pandey, *Food Technol. Biotechnol.*, 2006, **44**, 141–149.
36 Perstorp AB offers TMP in 20 and 50% renewable grade (Evyron™). (https://www.perstorp.com/en/products/proenvironment_polyols/evyron/).
37 F. P. Byrne, S. Jin, G. Paggiola, T. H. M. Petchey, J. H. Clark, T. J. Farmer, A. J. Hunt, C. R. McElroy and J. Sherwood, *Sustainable Chem. Processes*, 2016, **4**, 7.
38 B. Liu and S. Thayumanavan, *J. Am. Chem. Soc.*, 2017, **139**, 2306–2317.
39 P. J. Flory, *Principles of polymer chemistry*, Cornell University Press, San Diego, 1953.
40 J. Maul, B. G. Frushour, J. R. Kontoff, H. Eichenauer, K.-H. Ott and C. Schade, *Ullmann's Encyclopedia of Industrial Chemistry*, 2007, DOI: 10.1002/14356007.a21_615.pub2.
41 A. P. Pêgo, A. A. Poot, D. W. Grijpma and J. Feijen, *J. Mater. Sci.: Mater. Med.*, 2003, **14**, 767–773.
42 A. Yoshida, S. Honda, H. Goto and H. Sugimoto, *Polym. Chem.*, 2014, **5**, 1883–1890.
43 E. Gubbels, T. Heitz, M. Yamamoto, V. Chilekar, S. Zarbakhsh, M. Gepraegs, H. Köpnick, M. Schmidt, W. Brügging, J. Rüter and W. Kaminsky, *Ullmann's Encyclopedia of Industrial Chemistry*, 2018, DOI: 10.1002/14356007.a21_227.pub2.
44 G. Abts, T. Eckel and R. Wehrmann, *Ullmann's Encyclopedia of Industrial Chemistry*, 2014, DOI: 10.1002/14356007.a21_207.pub2.
45 G. Filippone, S. C. Carroccio, R. Mendichi, L. Gioiella, N. Tz. Dintcheva and C. Gambarotti, *Polymer*, 2015, **72**, 134–141.
46 J. A. Cadieux, D. J. Buller and P. D. Wilson, *Org. Lett.*, 2003, **5**, 3983–3986.

Supporting Information

Rigid biobased polycarbonates with good processability based on a spirocyclic diol derived from citric acid

Olivier Bonjour,† Ilme Liblikas,§ Tõnis Pehk,‡ Khai-Nghi Truong,‖ Kari Rissanen,‖ Lauri Vares,*,§ Patric Jannasch*,†,§

† Department of Chemistry, Lund University, Box 124, Lund 221 00, Sweden

§ Institute of Technology, University of Tartu, Nooruse 1, Tartu 50411, Estonia

‡ Laboratory of Chemical Physics, National Institute of Chemical Physics and Biophysics, Akadeemia tee 23, Tallinn 12618, Estonia

‖ University of Jyvaskyla, Department of Chemistry, P.O. Box 35, Survontie 9 B, Jyväskylä 40014, Finland

*E-mail: lauri.vares@ut.ee, patric.jannasch@chem.lu.se

Table of Contents

X-Ray crystallography

Single crystals of **3**-*trans* were measured using a dual-source Rigaku SuperNova diffractometer equipped with an Atlas detector and an Oxford Cryostream cooling system using Mo-K_α radiation (λ = 0.71073 Å). Data collection and reduction was performed using the program *CrysAlisPro*[1] and Gaussian face-index absorption correction method was applied.[1] The structure was solved with Direct Methods (*SHELXS*)[2] and refined by full-matrix least-squares based on F^2 using *SHELXL*-2015[2]. Non-hydrogen atoms were assigned anisotropic displacement parameters unless stated otherwise. Hydrogen atoms bonded to oxygens were located from Fourier difference maps and refined with an O-H distance restraint of approximately 0.92 Å; their site occupancies were constraint to 0.5. Other hydrogen atoms were placed in idealized positions and included as riding. Isotropic displacement parameters for all H atoms were constrained to multiples of the equivalent displacement parameters of their parent atoms with $U_{iso}(H) = 1.2\ U_{eq}$(parent atom). Several reflections with large discrepancies between the calculated and observed structure factors have been omitted from the least-squares refinement as outliers. In addition, enhanced rigid bond restraints[3] with standard uncertainties of 0.001 Å^2 were applied for several atom pairs as well as other restraints (DFIX, EXYZ, EADP). The disorders were refined to the respective two split positions (see below), with the sum of the site occupancies of both alternative positions constrained to unity. The crystal of **3**-*trans* proved to be a non-merohedral twin. In the twin refinement, an approximately modified set of intensity data taking the partially overlapped diffraction of a two-component twin into account (HKLF5 format in SHELXL-2015) gave significantly improved convergence results and relative domain fractions of 0.846 and 0.154 (before twin refinement: GooF = 2.428, R_1 = 0.1467, wR_2 = 0.3843, 0.568 <dΔρ < -0.426 eÅ^{-3}).

Crystal data for **3**-*trans* (obtained from slow evaporation of $CHCl_3$): CCDC- 1986990, $C_{20}H_{34}O_6$, M = 370.47 gmol^{-1}, colourless plate, 0.27 × 0.25 × 0.08 mm^3, monoclinic, space group $P2_1/n$ (No. 14), a = 7.8705(5) Å, b = 10.1489(7) Å, c = 23.9418(13) Å, α = 90°, β = 93.881(2)°, γ = 90°, V = 1908.0(2) Å^3, Z = 4, D_{calc} = 1.290 gcm^{-3}, F(000) = 808, μ = 0.094 mm^{-1}, T = 120(2) K, θ_{max} = 28.6°, 25408 total reflections, 2545 with $I_o > 2\sigma(I_o)$, R_{int} = 0.0755, 3560 data, 293 parameters, 55 restraints, GooF = 1.096, R_1 = 0.0997 and wR_2 = 0.2398 [$I_o > 2\sigma(I_o)$], R_1 = 0.1292 and wR_2 = 0.2549 (all reflections), 0.324 <dΔρ < -0.323 eÅ^{-3}.

X-ray structure of **3**-*trans* showing the major (59.3 %, solid lines) and the disordered, minor atom occupancies (40.7 %, dashed lines):[4]

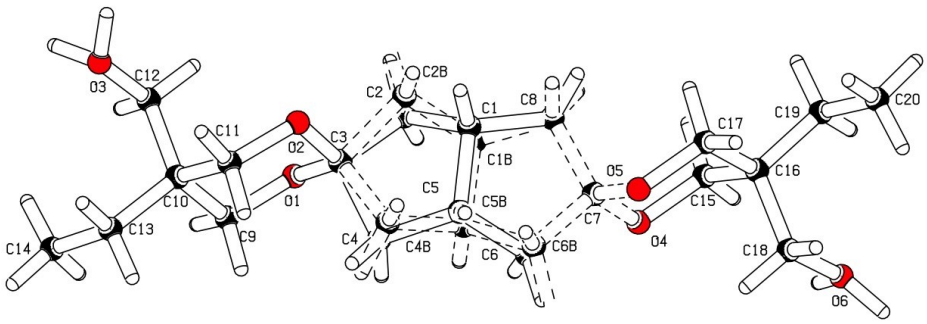

[1] Rigaku Oxford Diffraction, **2017**, *CrysAlisPro* software system, version 38.46, Rigaku Corporation, Oxford, UK.

[2] a) G. M. Sheldrick, *Acta Cryst.* **2008**, *A64*, 112–122.; b) G. M. Sheldrick, SHELXL13. Program package for crystal structure determination from single crystal diffraction data, University of Göttingen, Germany, 2013.; c) G. M. Sheldrick, *Acta Cryst.* **2015**, *C71*, 3–8.

[3] a) F. L. Hirshfeld, *Acta Cryst.* **1976**, *A32*, 239–244.; b) A. Thorn, B. Dittrich, G. M. Sheldrick, *Acta Cryst*. **2012**, *A68*, 448–451.

[4] A. L. Spek, *Acta Cryst*. **2009**, *D65*, 148–155.

Table S1. ^{1}H and ^{13}C NMR chemical shifts of **3**-*cis*, **3**-*trans* and **PC**-*h* in $CDCl_3$ at 288 K.

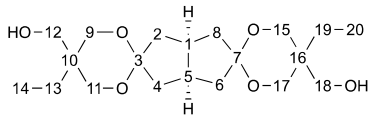

subunit		Bicyclo[3.3.0]octane ring			Dioxane ring		Ethyl		CH_2 OH	
atoms		1,5	2,4,6,8	3,7	9,11,15,17	10,16	14,20	13,19	12,18	OH
trans	^{1}H	2.54 m	n 1.71, 1.74* x 2.07, 2.30*	-	a 3.55, 3.57*, e 3.70, 3.69*	-	0.82	1.26	3.77bs	2.07bs
	^{13}C	36.82	43.39 35.95*	110.18	67.04 66.32*	36.74	6.93	23.68	62.62	-
cis	^{1}H	2.55m 2.52*m	n 1.69*, 1.74 x 2.30*, 2.08	-	a 3.55, 3.57* e 3.71, 3.69*	-	0.83	1.29	3.73 3.74	2.11bs
	^{13}C	37.98 35.68*	42.95 36.45*	110.19	67.01 66.27*	36.81	7.00	23.65	62.66	-
poly-mer**	^{1}H	2.58-2.49m	n 1.75-1.67 x 2.30-2.26 x 2.11-2.07	-	3.70-3.68, 3.58-3.55	-	0.81, 0.82	1.33, 1.29	4.32-4.24	-
	^{13}C	37.93c,36.82t, 35.74c	43.34, 42.70, 36.60, 35.91	110.30 110.28	66.70, 66.01, 65.92	35.88 35.87, 35.82	6.93, 6.84,	23.59, 23.54	67.27, 67.25, 67.19, 67.17	-

* Denotes geminal protons and connected to them carbon atoms; m- unresolved multiplet, bs- broad singlet, n-*endo*, x- *exo*, a-axial, e- equatorial. ** OCOO carbons at 155.34(1),155.31(2) and 155.28(1) ppm. Spin-spin coupling constants from pseudo first order spectra: in *trans* isomer for bicyclo[3.3.0]octane ring H-2,4,6,8 *endo* protons ddd 13.3, 6.1 and 1.2 Hz, *exo* protons ddd 13.3, 8.9 and 1.8 Hz; in *cis* isomer *endo* protons ddd 13.3, 6.8 and 0.9 Hz, *exo* protons ddd 13.3, 8.7 and 1.8 Hz; in dioxane ring of *trans* isomer axial H d 11.8 Hz, equatorial H dd 11.8 and 2.0 Hz, in *cis* isomer axial H d 11.7 Hz, equatorial H dd 11.7 and 1.9 Hz.

Table S2. Optimization of the ketalization reaction between diketone **1** and TMP **2** to afford spiro-diol **3**.

Entry	TMP (equiv.)	Catalyst (mol%)	Solvent	Reflux time (h)	Extraction (yes/no)	Purification method	Yield (%)	Comment
1	3	5	Toluene	6	no	chromatography	68	Incomplete conversion
2	4	10	Toluene	36	no	chromatography	78	Turned very dark
3	6	5	cHex:DMF (1:4)	48	no	chromatography	84	Complete conversion, some dark solids formed
4	3	5	cHex:DMF (1:4)	6	yes	crystallization	70	
5	2.6	5	cHex:DMF (1:4)	6	no	chromatography	69	
6	3.5	1	cHex:DMF (1:4)	8	yes	crystallization	85	
7	3.5	1	cHex:DMF (1:4)	20	yes	chromatography	55	Some dark solids formed
8	**3.5**	**1**	**cHex:DMF (1:4)**	**8**	**no**	**chromatography**	**91**	***Reported in the paper***
9	2.2	1	cHex:Tol (3:2)	8	no	crystallization		Incomplete conversion, Traces of TMP in product
10	1.95	1	cHex:Tol (3:2)	20	no	crystallization	76	Incomplete conversion
11	**2.2**	**1**	**cHex:Tol (3:2)**	**16**	**no**	**Crystallized twice**	**85/74 ***	***Reported in the paper***

* To remove small residues of TMP, product (**3**) was dissolved in EtOAc and recrystallized to yield 74% of pure product.

Table S3. Optimization of polycondensation conditions.

Entry	DPC : **3** (ratio)	Catalyst	Initial temp. (°C)	Time at 160 °C (min)	Final temp. (°C)	Time at final temp. (min)	Yield (%)	M_n (kg mol^{-1})	$Đ$	Polycondensation conditions and comments (see below table)
1	1.1 : 1.0	LiAcac	120	40	230	50	88	6.5	5.79	a
2	1.1 : 1.0	LiAcac	120	40	210	20	87	4.9	4.45	b
3	1.1 : 1.0	LiAcac	120	40	210	50	78	5.5	4.56	c
4	1.1 : 1.0	$NaHCO_3$	120	180	260	10	70	8.0	6.34	d
5	1.0 : 1.0	$NaHCO_3$	160	30	250	30	84	5.0	2.87	e
6	1.0 : 1.0	$NaHCO_3$	120	30	260	10	68	2.7	2.14	f
7	1.1 : 1.0	$NaHCO_3$	160	80	260	10	59	2.6	1.89	g
8	1.1 : 1.0	$NaHCO_3$	160	80	260	60	69	3.5	2.61	h
9 (PC-*h*)	1.1 : 1.0	$NaHCO_3$	160	110	280	60	90	27.7	3.40	Reported in the paper
10 (PC-*l*)	1.1 : 1.0	$NaHCO_3$	120	120	210	15	86	7.5	3.55	Reported in the paper

Conditions:

a) The reaction mixture was melted and degassed at 120 °C. After 1 h the temperature was increased to 160 °C during 2 h and during the last 1.5 h the pressure was gradually reduced to 50 mbar. After heating at 160 °C for 40 min, the temperature of the reaction mixture was increased to 230 °C during 2 h. At the same time the pressure was reduced to 0.3 mbar. After 50 min, the product was cooled, dissolved and precipitated.

b) Similar as (a) but the final heating lasted 20 min at 210 °C.

c) Similar as (a) but the final heating lasted 50 min at 210 °C.

d) The reaction mixture was melted and degassed at 120 °C. After 60 min, it was heated to 160 °C and was kept at this temperature for 3 h. During the second and third hour at 160 °C, the pressure was gradually reduced from 300 to 100 mbar. Next, the temperature was raised to 220 °C at a rate of 1 °C min^{-1} while the pressure was reduced to 50 mbar. Finally, the temperature was increased to 260 °C and the pressure reduced to 0.3 mbar during 20 min. After 10 min the reaction was stopped.

e) The reaction mixture was melted and degassed at 160 °C. After 30 min, the heating was started and the reaction mixture was heated to 200 °C during 1 h. Then it was heated to 220 °C during 45 min and the pressure was reduced to 200 mbar. While keeping temperature at 220 °C during 45 min, the pressure was reduced to 10 mbar. Over 15 min the temperature was increased to 250 °C, and after 30 min the product was cooled, dissolved and precipitated.

f) The procedure started just as (a). In contrast, it was kept at 160 °C only for 30 min and thereafter heated to 220 °C at a rate of 1 °C min^{-1} while the pressure was reduced to 50 mbar. Finally, the temperature was raised to 260 °C and the pressure reduced to 0.3 mbar during 20 min. After 10 min the reaction was stopped.

g) The reaction mixture was melted and degassed at 160 °C. After 80 min the heating was started and the reaction mixture was heated to 260 °C during 2.5 h. At the same time, the pressure was reduced to 0.32 mbar at a constant rate. Finally, the reaction mixture was kept at 260 °C and 0.32 mbar for 10 min.

h) Procedure (g) was followed, but the final heating was extended to 60 min.

General trends and observations:

1. The use of $NaHCO_3$ as catalyst seemed to yield PCs with higher MW compared to those prepared using LiAcac.

2. Variation of the stoichiometry of the starting materials showed that improved results were obtained when 1.1 equivalents of diphenylcarbonate was used per 1 equivalent of diol.

3. Starting the polycondensation at a lower temperature (120 °C) did not appear to improve the outcome, since higher MW polymers were not obtained. The optimum starting temperature seemed to be 160 °C. Longer reaction time at 160 °C gave better results compared experiments where reaction mixture was heated up more quickly.

4. A higher reaction temperature and longer time at the final temperature resulted products with increased MWs.

5. Shorter reaction times gave products with lower MWs and lower yields despite the high final temperature.

6. It was necessary to reduce the pressure of the reaction mixture gradually to 0.3 mbar. In general, the polycondensation was stopped when the reaction mixture began to darken markedly, or had become so viscous that no further agitation was observed.

^{1}H and ^{13}C NMR spectra

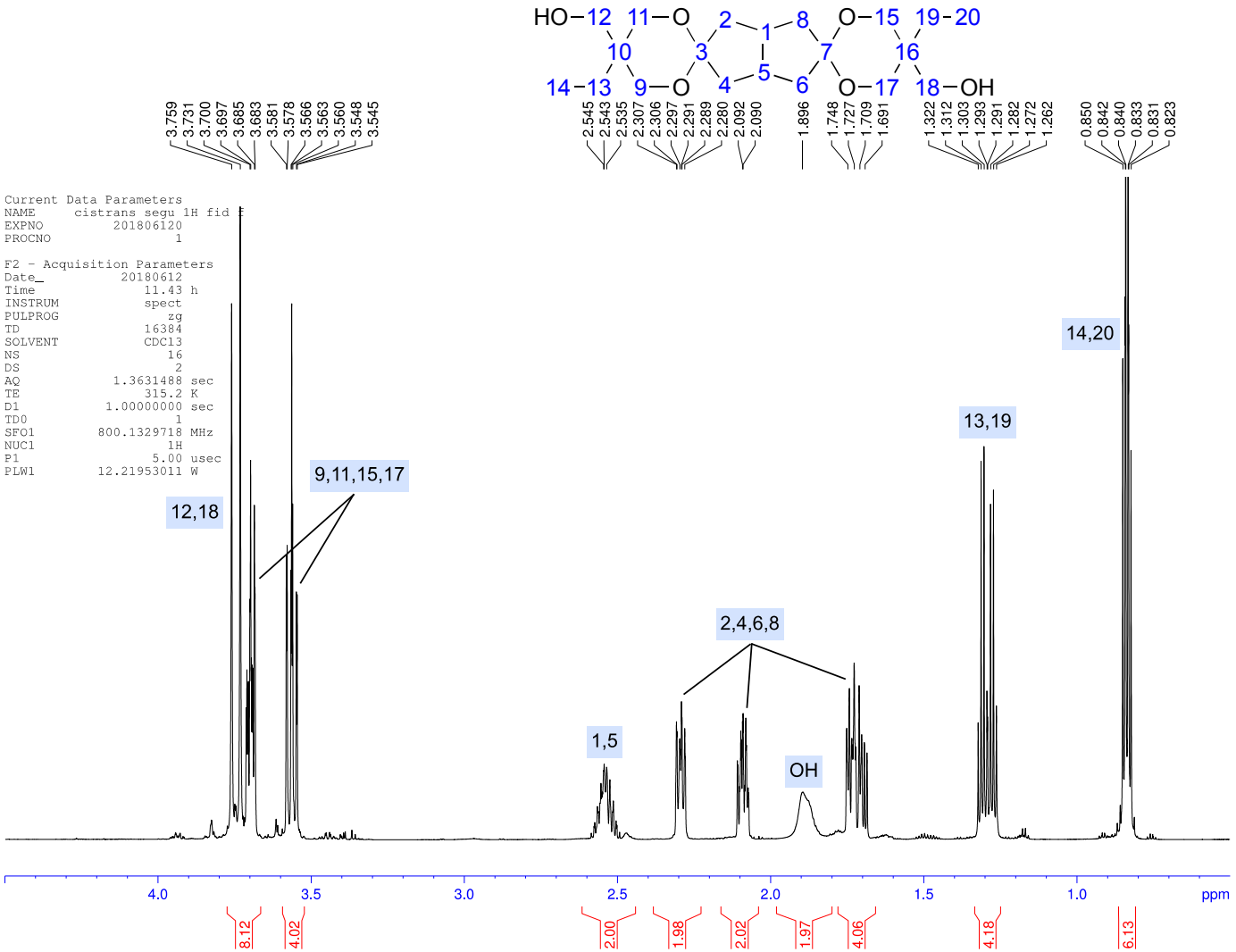
HO–12 11–O 2 1 8 O–15 19–20
10 3 7 16
14–13 9–O 4 5 6 O–17 18–OH
3.759 3.731 3.700 3.697 3.685 3.683 3.581 3.578 3.566 3.563 3.560 3.548 3.545
2.545 2.543 2.535 2.307 2.306 2.297 2.291 2.289 2.280 2.092 2.090 1.896 1.748 1.727 1.709 1.691 1.322 1.312 1.303 1.293 1.291 1.282 1.272 1.262 0.850 0.842 0.840 0.833 0.831 0.823
Current Data Parameters
NAME cistrans segu 1H fid E
EXPNO 201806120
PROCNO 1
F2 - Acquisition Parameters
Date_ 20180612
Time 11.43 h
INSTRUM spect
PULPROG zg
TD 16384
SOLVENT CDCl3
NS 16
DS 2
AQ 1.3631488 sec
TE 315.2 K
D1 1.00000000 sec
TD0 1
SFO1 800.1329718 MHz
NUC1 1H
P1 5.00 usec
PLW1 12.21953011 W
12,18
9,11,15,17
1,5
2,4,6,8
OH
13,19
14,20
4.0 3.5 3.0 2.5 2.0 1.5 1.0 ppm
8.12 4.02 2.00 1.98 2.02 1.97 4.06 4.18 6.13

Figure S1. ^{1}H NMR spectrum of the **3**-*cis*/*trans* monomer mixture.

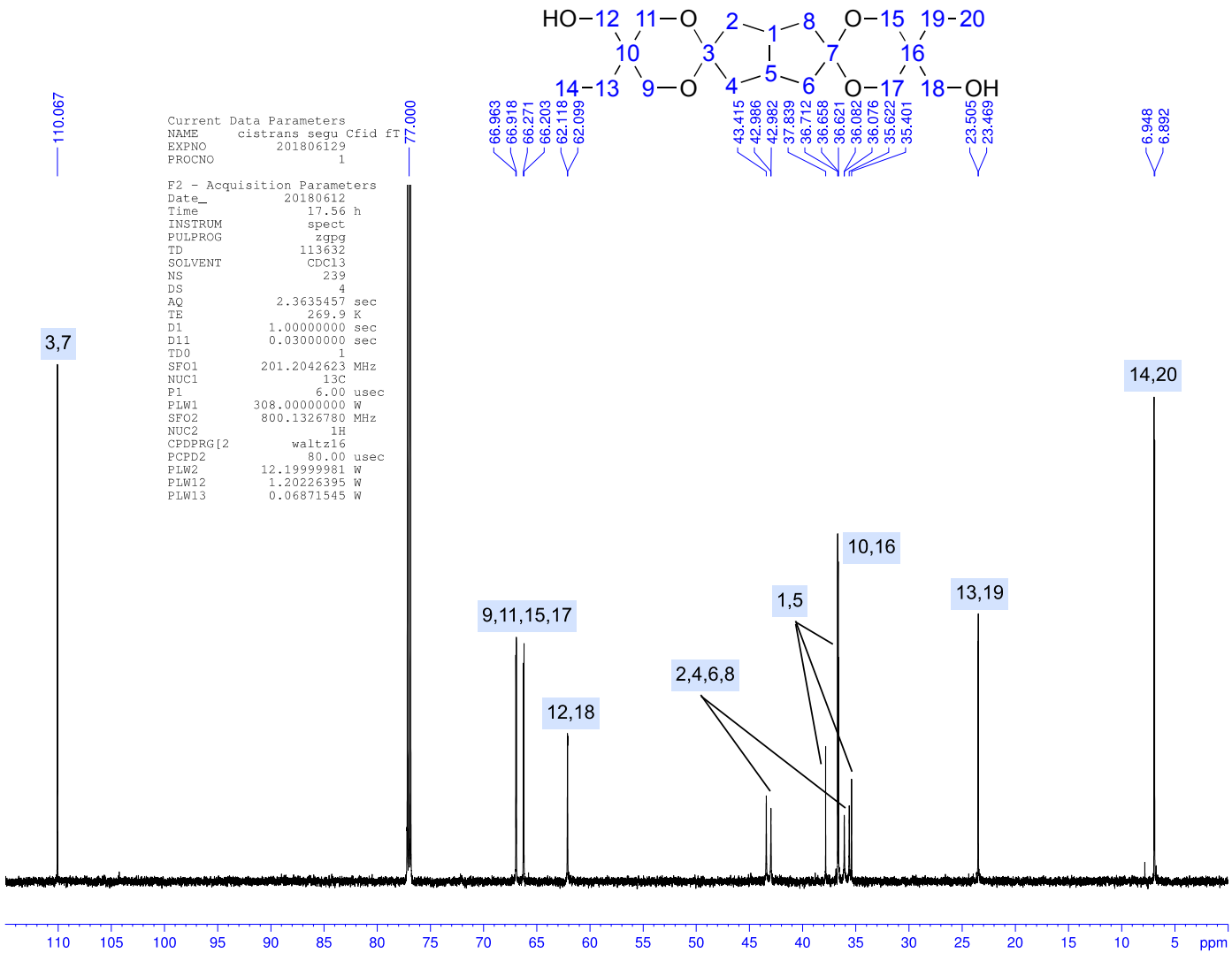
HO−12 11−O 2 1 8 O−15 19-20
10 3 5 7 16
14−13 9−O 4 6 O−17 18−OH
110.067
77.000
66.963
66.918
66.271
66.203
62.118
62.099
43.415
42.986
42.982
37.839
36.712
36.658
36.621
36.082
36.076
35.622
35.401
23.505
23.469
6.948
6.892
3,7
14,20
10,16
1,5
13,19
9,11,15,17
2,4,6,8
12,18
Current Data Parameters
NAME cistrans segu Cfid fT
EXPNO 201806129
PROCNO 1
F2 - Acquisition Parameters
Date_ 20180612
Time 17.56 h
INSTRUM spect
PULPROG zgpg
TD 113632
SOLVENT CDCl3
NS 239
DS 4
AQ 2.3635457 sec
TE 269.9 K
D1 1.00000000 sec
D11 0.03000000 sec
TD0 1
SFO1 201.2042623 MHz
NUC1 13C
P1 6.00 usec
PLW1 308.00000000 W
SFO2 800.1326780 MHz
NUC2 1H
CPDPRG[2 waltz16
PCPD2 80.00 usec
PLW2 12.19999981 W
PLW12 1.20226395 W
PLW13 0.06871545 W
110 105 100 95 90 85 80 75 70 65 60 55 50 45 40 35 30 25 20 15 10 5 ppm

Figure S2. ^{13}C NMR spectrum of the **3**-*cis*/*trans* monomer mixture.

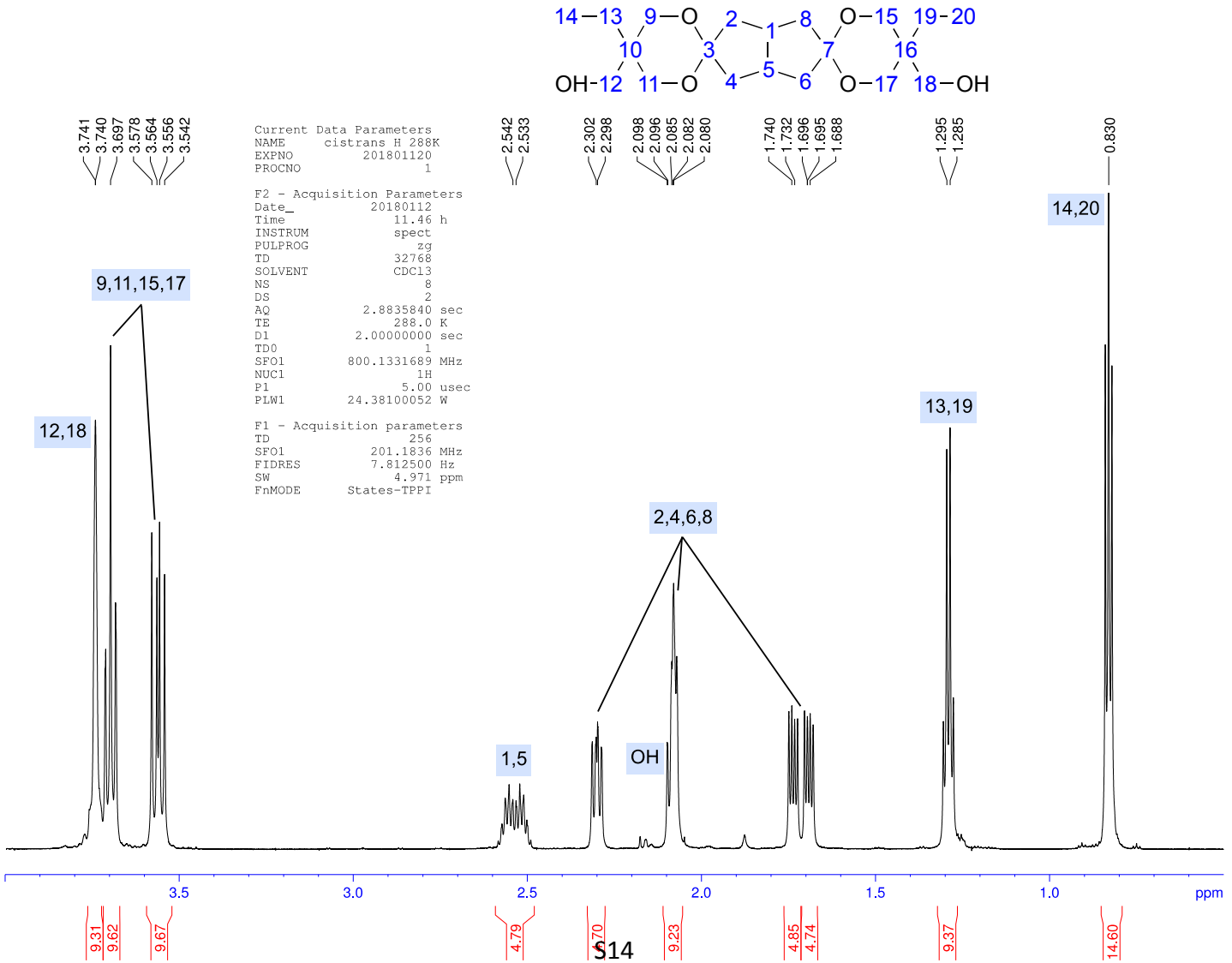
14–13 9–O 2 1 8 O–15 19–20
10 3 5 7 16
OH–12 11–O 4 6 O–17 18–OH
3.741
3.740
3.697
3.578
3.564
3.556
3.542
2.542
2.533
2.302
2.298
2.098
2.096
2.085
2.082
2.080
1.740
1.732
1.696
1.695
1.688
1.295
1.285
0.830
Current Data Parameters
NAME cistrans H 288K
EXPNO 201801120
PROCNO 1
F2 - Acquisition Parameters
Date_ 20180112
Time 11.46 h
INSTRUM spect
PULPROG zg
TD 32768
SOLVENT CDCl3
NS 8
DS 2
AQ 2.8835840 sec
TE 288.0 K
D1 2.00000000 sec
TD0 1
SFO1 800.1331689 MHz
NUC1 1H
P1 5.00 usec
PLW1 24.38100052 W
F1 - Acquisition parameters
TD 256
SFO1 201.1836 MHz
FIDRES 7.812500 Hz
SW 4.971 ppm
FnMODE States-TPPI
9,11,15,17
12,18
14,20
13,19
2,4,6,8
1,5
OH
3.5
3.0
2.5
2.0
1.5
1.0
ppm
9.31
9.62
9.67
4.79
4.70
9.23
4.85
4.74
9.37
14.60

Figure S3. ^{1}H NMR spectrum of the **3**-*cis* monomer in $CDCl_3$.

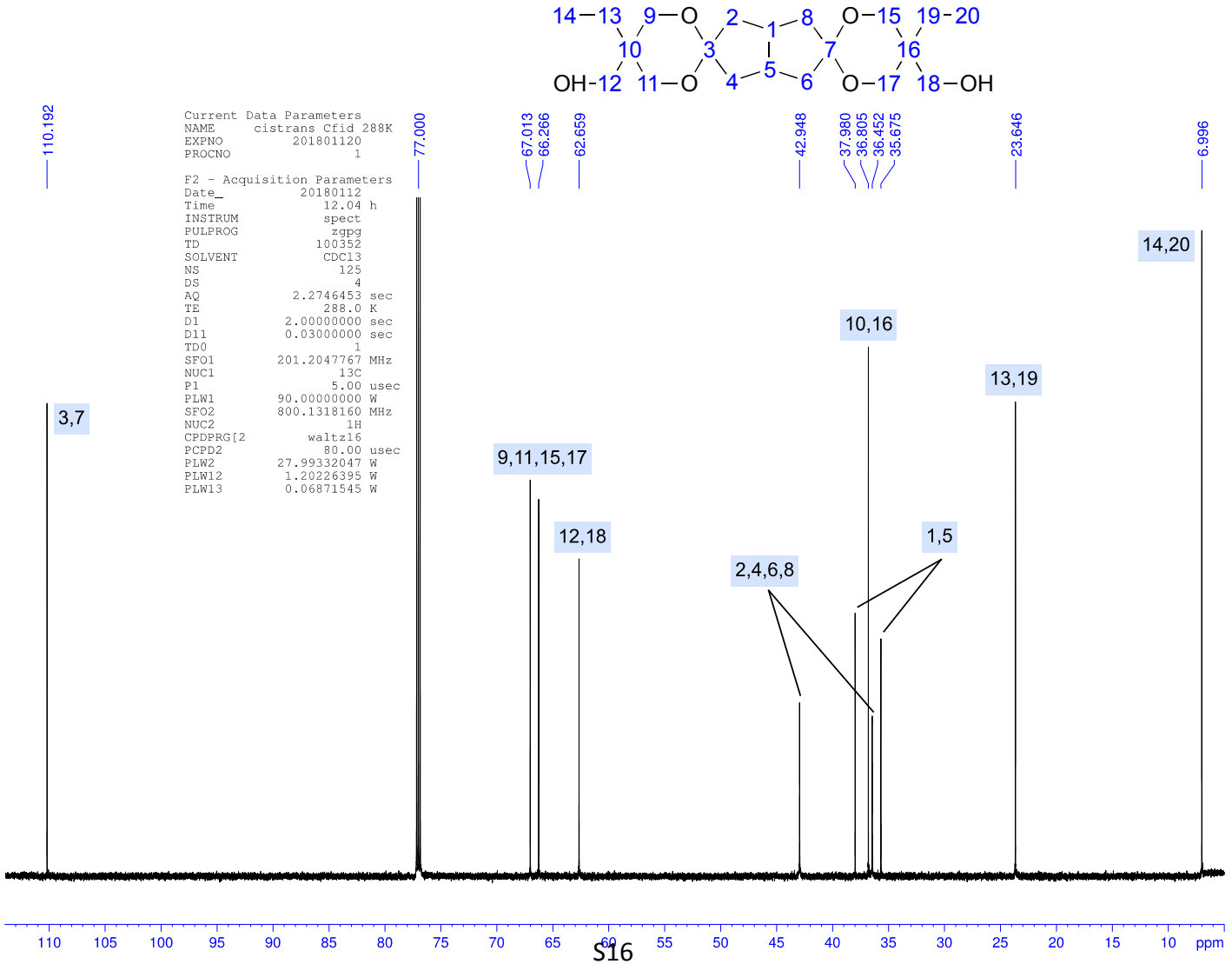
14–13 9–O 2 1 8 O–15 19-20
10 3 7 16
OH-12 11–O 4 5 6 O–17 18–OH
110.192
77.000
67.013
66.266
62.659
42.948
37.980
36.805
36.452
35.675
23.646
6.996
Current Data Parameters
NAME cistrans Cfid 288K
EXPNO 201801120
PROCNO 1
F2 - Acquisition Parameters
Date_ 20180112
Time 12.04 h
INSTRUM spect
PULPROG zgpg
TD 100352
SOLVENT CDCl3
NS 125
DS 4
AQ 2.2746453 sec
TE 288.0 K
D1 2.00000000 sec
D11 0.03000000 sec
TD0 1
SFO1 201.2047767 MHz
NUC1 13C
P1 5.00 usec
PLW1 90.00000000 W
SFO2 800.1318160 MHz
NUC2 1H
CPDPRG[2 waltz16
PCPD2 80.00 usec
PLW2 27.99332047 W
PLW12 1.20226395 W
PLW13 0.06871545 W
3,7
9,11,15,17
12,18
2,4,6,8
10,16
1,5
13,19
14,20
110 105 100 95 90 85 80 75 70 65 60 55 50 45 40 35 30 25 20 15 10 ppm

Figure S4. ^{13}C NMR spectrum of the **3**-*cis*-monomer in $CDCl_3$.

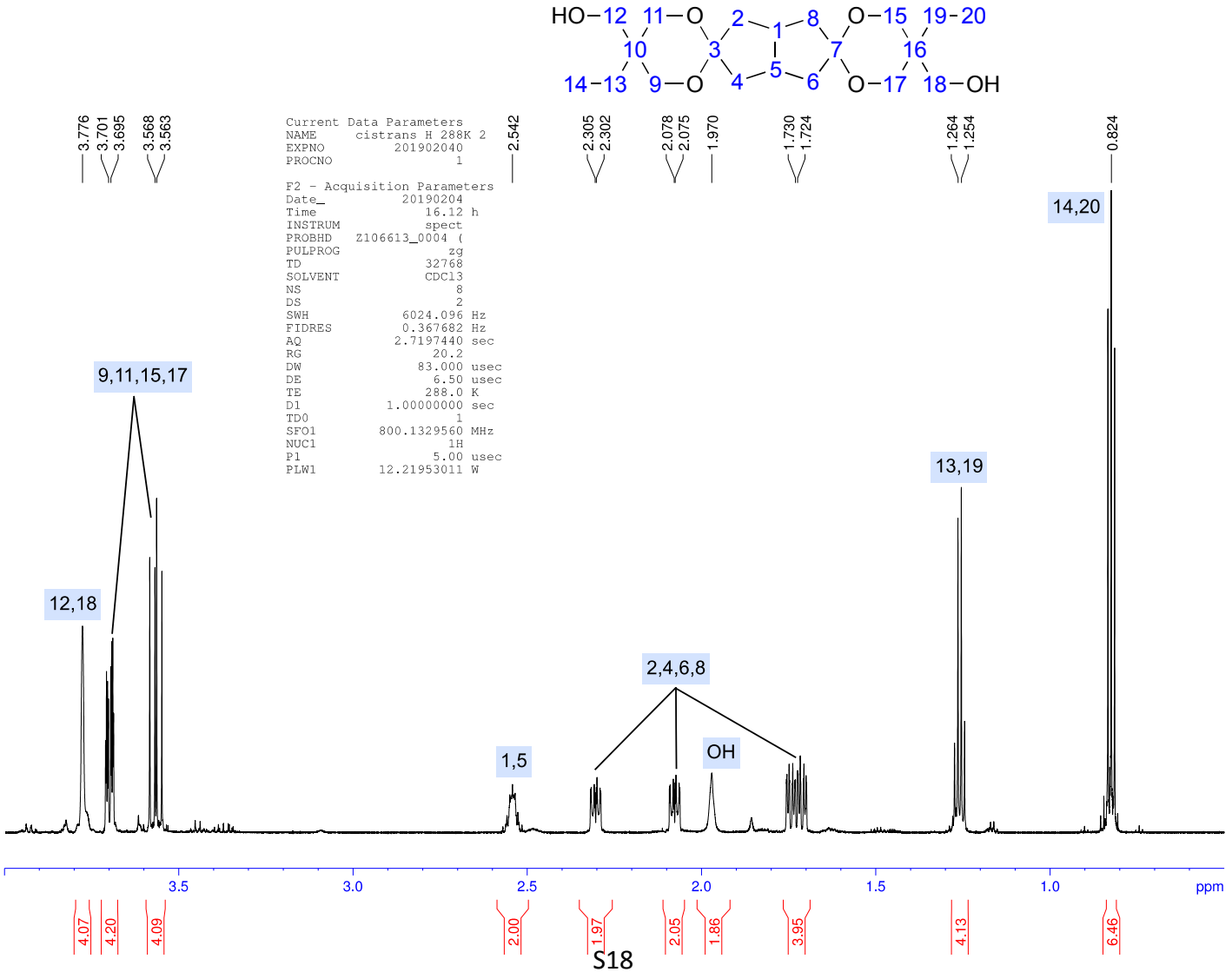
HO−12 11−O 2 1 8 O−15 19-20
10 3 7 16
14−13 9−O 4 5 6 O−17 18−OH
3.776
3.701
3.695
3.568
3.563
2.542
2.305
2.302
2.078
2.075
1.970
1.730
1.724
1.264
1.254
0.824
Current Data Parameters
NAME cistrans H 288K 2
EXPNO 201902040
PROCNO 1
F2 - Acquisition Parameters
Date_ 20190204
Time 16.12 h
INSTRUM spect
PROBHD Z106613_0004 (
PULPROG zg
TD 32768
SOLVENT CDCl3
NS 8
DS 2
SWH 6024.096 Hz
FIDRES 0.367682 Hz
AQ 2.7197440 sec
RG 20.2
DW 83.000 usec
DE 6.50 usec
TE 288.0 K
D1 1.00000000 sec
TD0 1
SFO1 800.1329560 MHz
NUC1 1H
P1 5.00 usec
PLW1 12.21953011 W
9,11,15,17
12,18
1,5
2,4,6,8
OH
13,19
14,20
3.5
3.0
2.5
2.0
1.5
1.0
ppm
4.07
4.20
4.09
2.00
1.97
2.05
1.86
3.95
4.13
6.46

Figure S5. ^{1}H NMR spectrum of the **3**-*trans* monomer in $CDCl_3$.

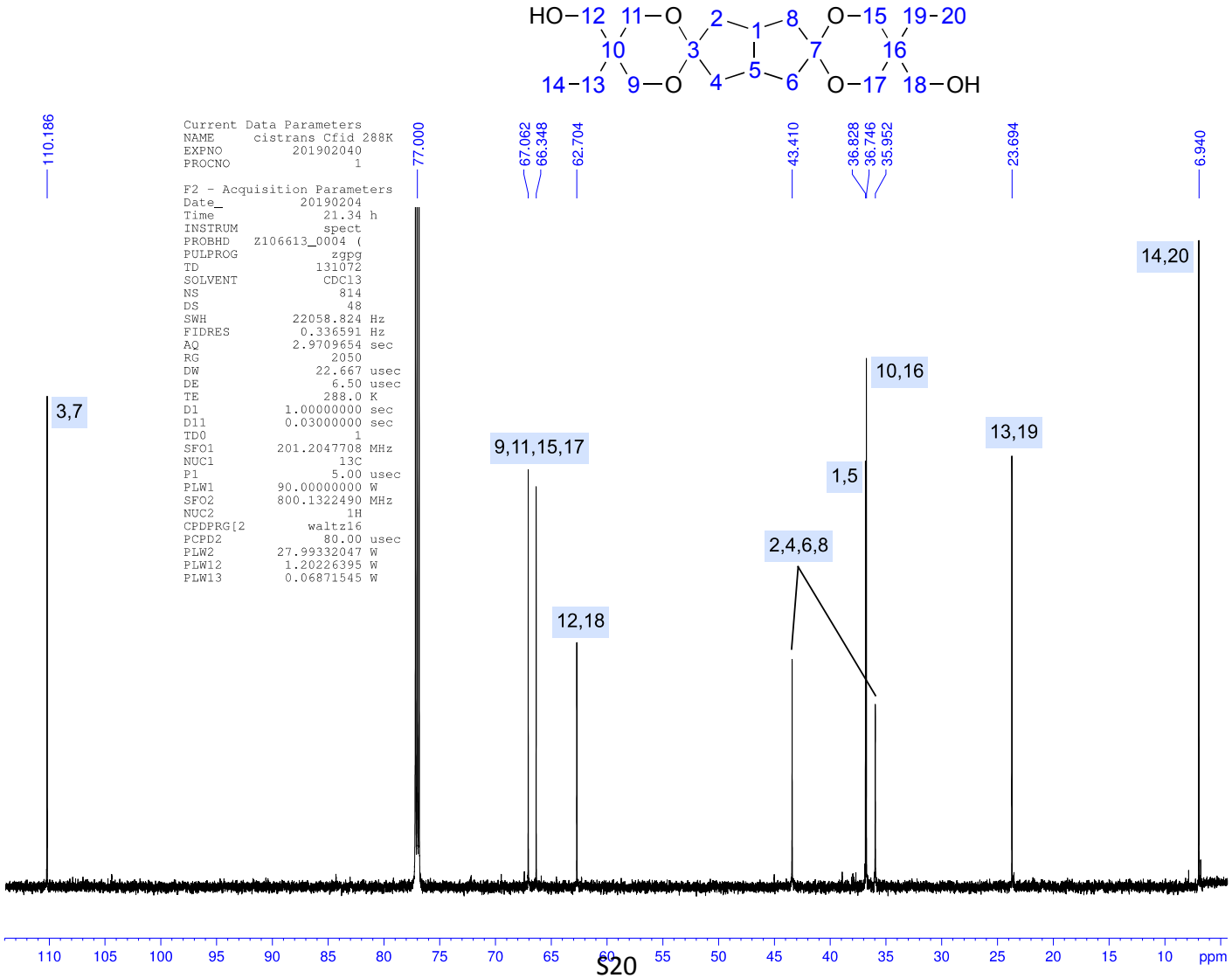
HO–12 11–O 2 1 8 O–15 19-20
10 3 7 16
14–13 9–O 4 5 6 O–17 18–OH
110.186
77.000
67.062
66.348
62.704
43.410
36.828
36.746
35.952
23.694
6.940
Current Data Parameters
NAME cistrans Cfid 288K
EXPNO 201902040
PROCNO 1
F2 - Acquisition Parameters
Date_ 20190204
Time 21.34 h
INSTRUM spect
PROBHD Z106613_0004 (
PULPROG zgpg
TD 131072
SOLVENT CDCl3
NS 814
DS 48
SWH 22058.824 Hz
FIDRES 0.336591 Hz
AQ 2.9709654 sec
RG 2050
DW 22.667 usec
DE 6.50 usec
TE 288.0 K
D1 1.00000000 sec
D11 0.03000000 sec
TD0 1
SFO1 201.2047708 MHz
NUC1 13C
P1 5.00 usec
PLW1 90.00000000 W
SFO2 800.1322490 MHz
NUC2 1H
CPDPRG[2 waltz16
PCPD2 80.00 usec
PLW2 27.99332047 W
PLW12 1.20226395 W
PLW13 0.06871545 W
3,7
9,11,15,17
12,18
2,4,6,8
1,5
10,16
13,19
14,20
110 105 100 95 90 85 80 75 70 65 60 55 50 45 40 35 30 25 20 15 10 ppm

Figure S6. ^{13}C NMR spectrum of the **3**-*trans* monomer in $CDCl_3$.

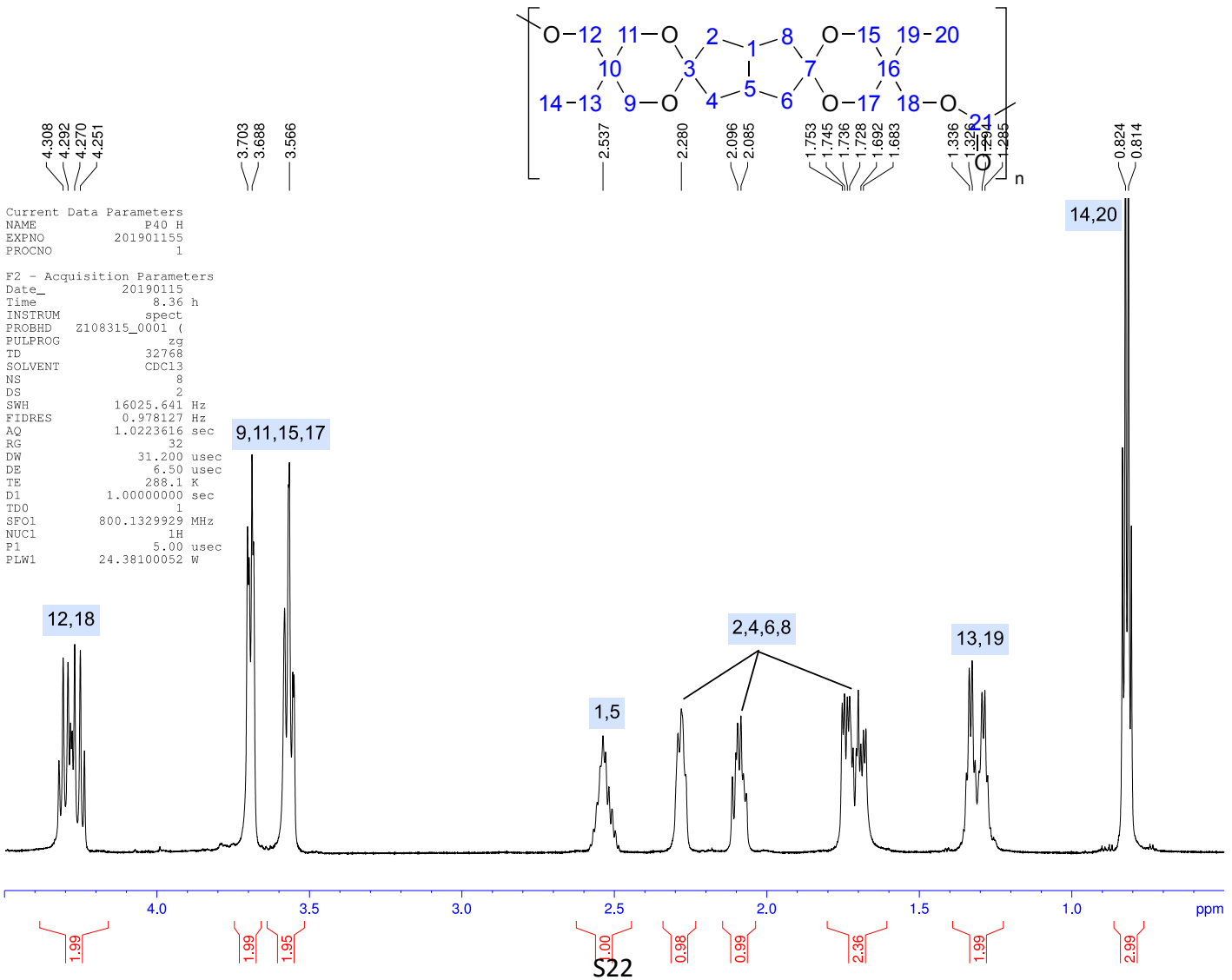
4.308
4.292
4.270
4.251
3.703
3.688
3.566
2.537
2.280
2.096
2.085
1.753
1.745
1.736
1.728
1.692
1.683
1.336
1.326
1.294
1.285
0.824
0.814
n
Current Data Parameters
NAME P40 H
EXPNO 201901155
PROCNO 1
F2 - Acquisition Parameters
Date_ 20190115
Time 8.36 h
INSTRUM spect
PROBHD Z108315_0001 (
PULPROG zg
TD 32768
SOLVENT CDCl3
NS 8
DS 2
SWH 16025.641 Hz
FIDRES 0.978127 Hz
AQ 1.0223616 sec
RG 32
DW 31.200 usec
DE 6.50 usec
TE 288.1 K
D1 1.00000000 sec
TD0 1
SFO1 800.1329929 MHz
NUC1 1H
P1 5.00 usec
PLW1 24.38100052 W
12,18
9,11,15,17
1,5
2,4,6,8
13,19
14,20
4.0
3.5
3.0
2.5
2.0
1.5
1.0
ppm
1.99
1.99
1.95
3.00
0.98
0.99
2.36
1.99
2.99

Figure S7. ^{1}H NMR spectrum of spiro-polymer **PC**-*h* in $CDCl_3$.

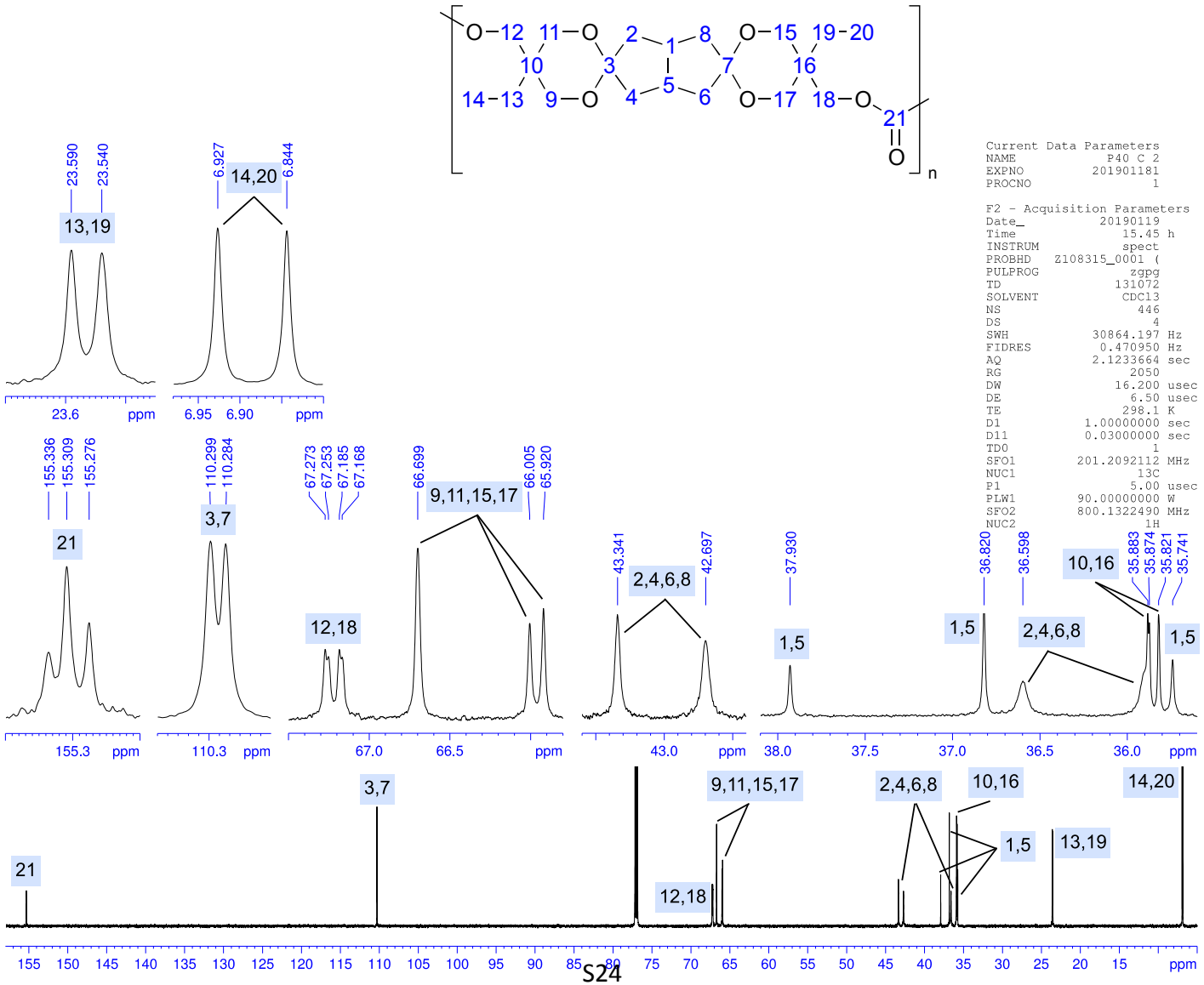
O–12 11–O 2 1 8 O–15 19–20
10 3 7 16
14–13 9–O 4 5 6 O–17 18–O 21
O
n
23.590
23.540
13,19
6.927
14,20
6.844
155.336
155.309
155.276
21
110.299
110.284
3,7
67.273
67.253
67.185
67.168
12,18
66.699
9,11,15,17
66.005
65.920
43.341
2,4,6,8
42.697
37.930
1,5
36.820
36.598
1,5
2,4,6,8
10,16
35.883
35.874
35.821
35.741
1,5
Current Data Parameters
NAME P40 C 2
EXPNO 201901181
PROCNO 1
F2 - Acquisition Parameters
Date_ 20190119
Time 15.45 h
INSTRUM spect
PROBHD Z108315_0001 (
PULPROG zgpg
TD 131072
SOLVENT CDC13
NS 446
DS 4
SWH 30864.197 Hz
FIDRES 0.470950 Hz
AQ 2.1233664 sec
RG 2050
DW 16.200 usec
DE 6.50 usec
TE 298.1 K
D1 1.00000000 sec
D11 0.03000000 sec
TD0 1
SFO1 201.2092112 MHz
NUC1 13C
P1 5.00 usec
PLW1 90.00000000 W
SFO2 800.1322490 MHz
NUC2 1H
21
3,7
12,18
9,11,15,17
2,4,6,8
10,16
1,5
13,19
14,20
ppm

Figure S8. ^{13}C NMR spectrum of **PC**-*h* spiro-polymer in $CDCl_3$.

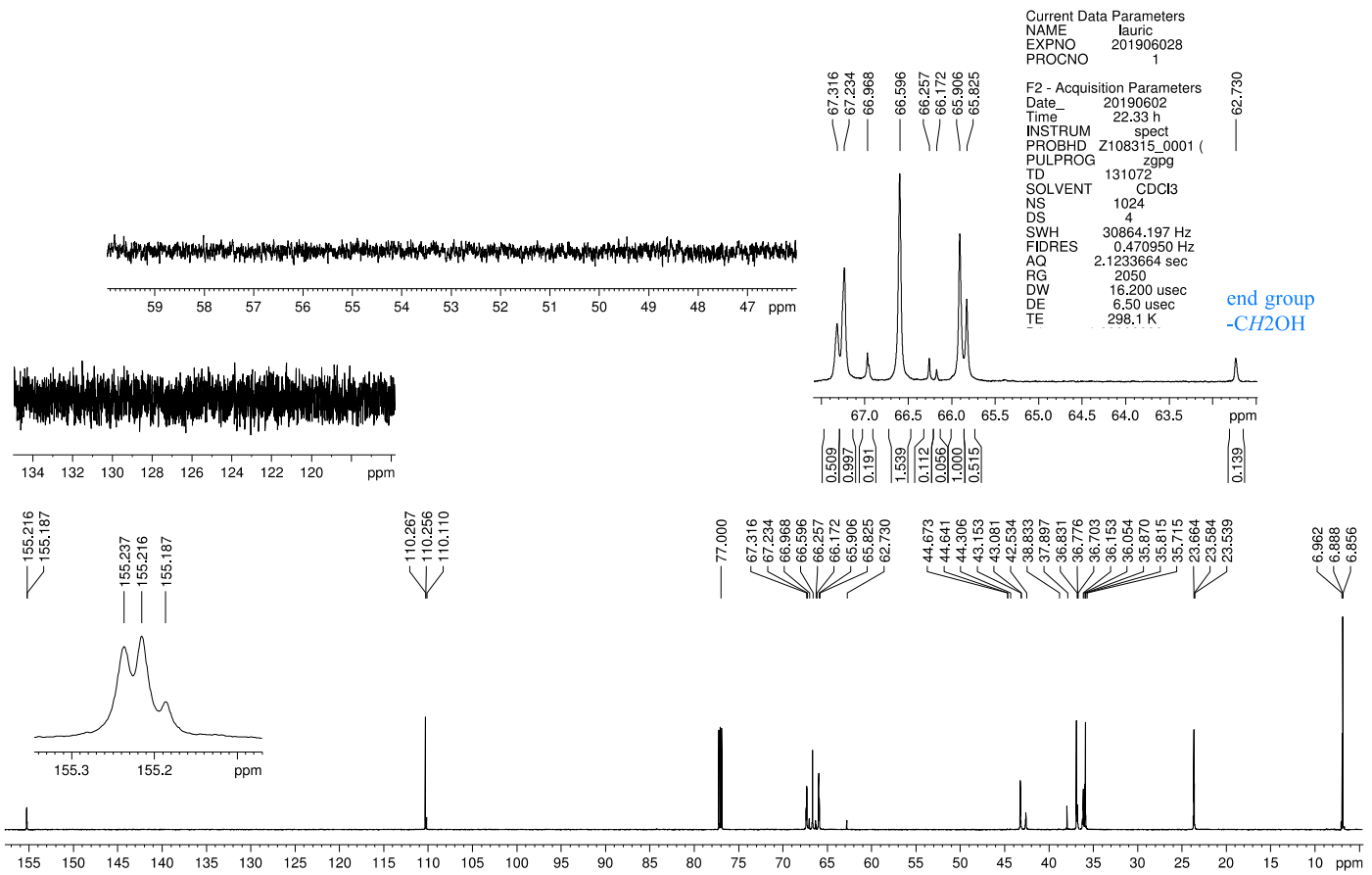

Figure S9. End group analysis of **PC-*l*** by ^{13}C NMR spectroscopy.

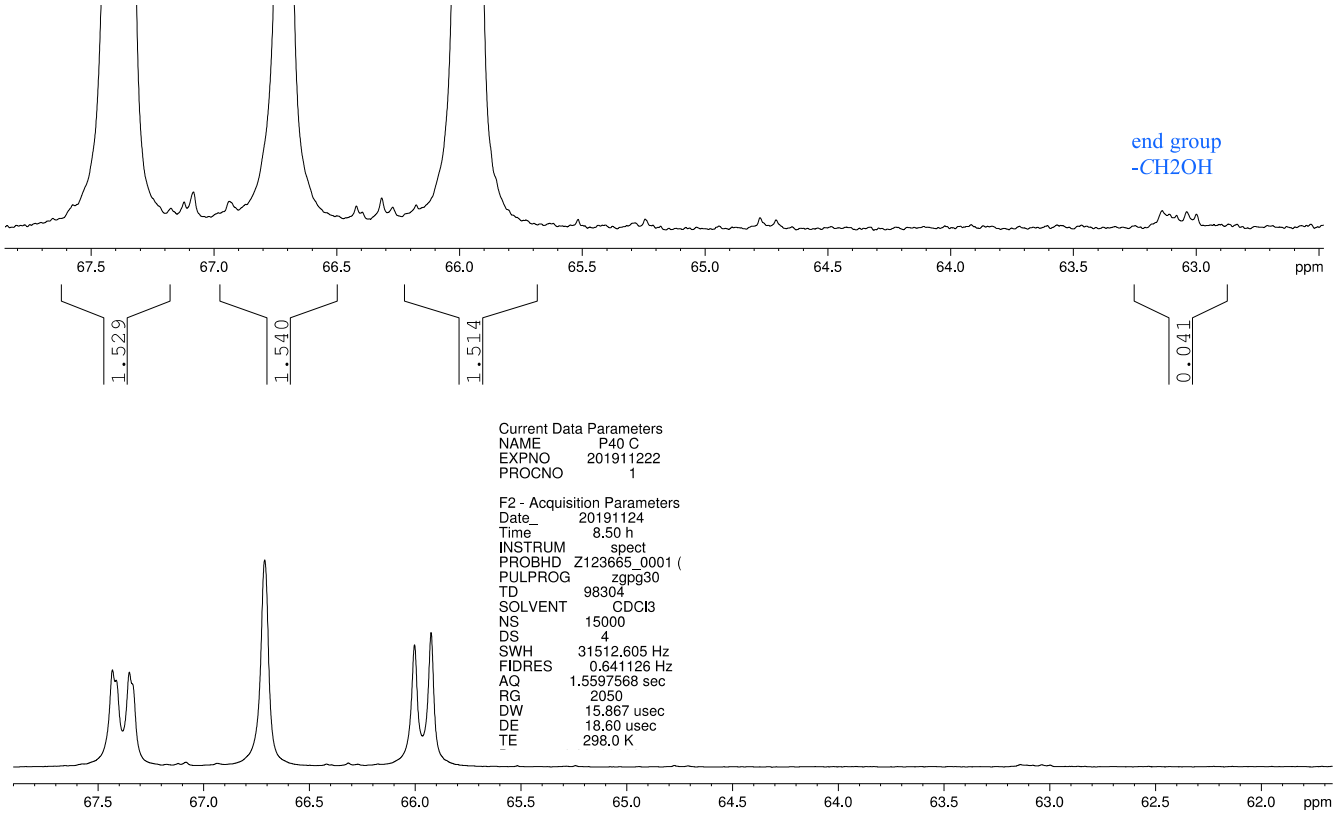

Figure S10. End group analysis of **PC**-*h* by ^{13}C NMR spectroscopy.

Hydrolysis of spiro-diol 3

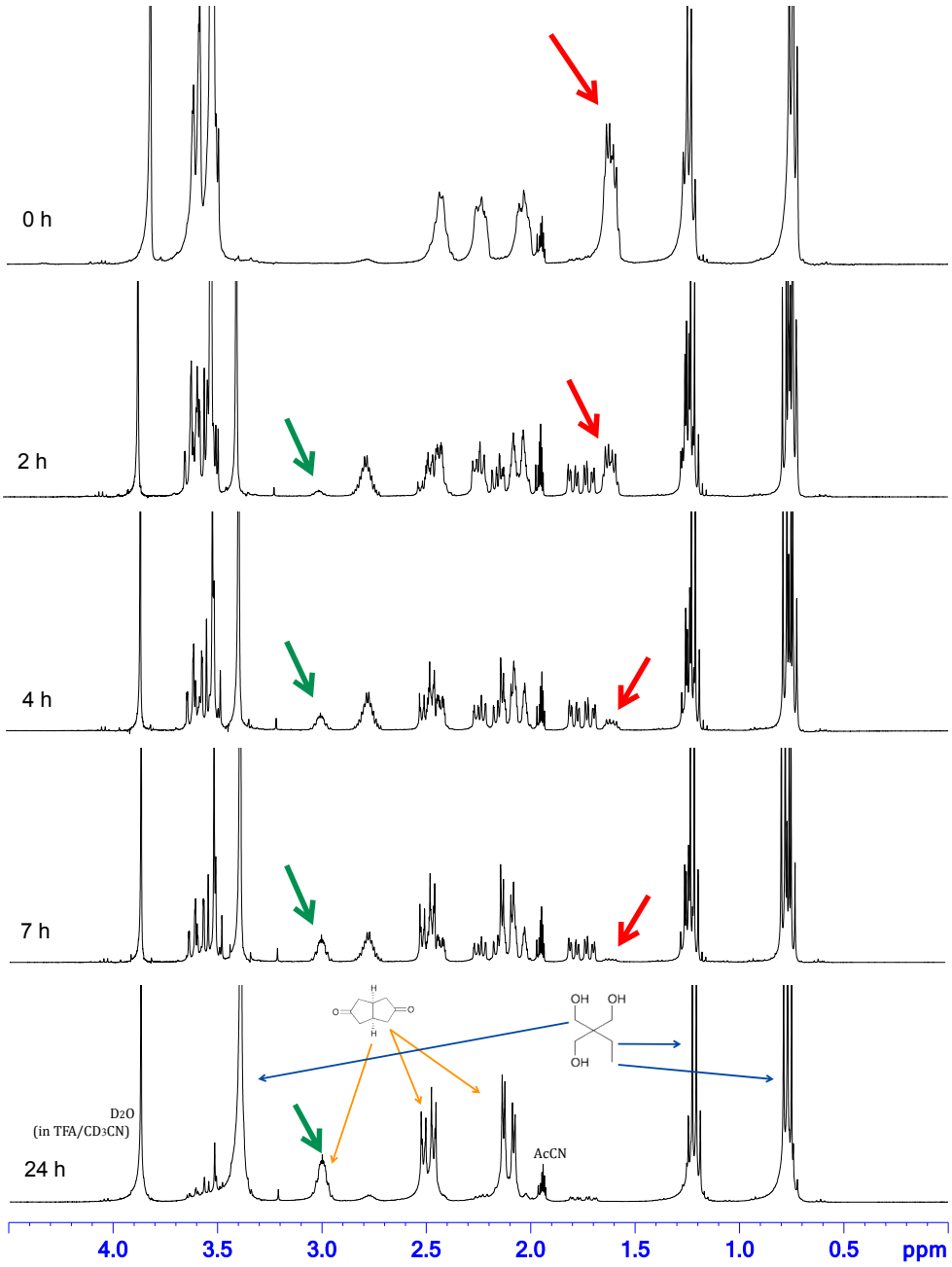

Figure S11. ^{1}H NMR spectra of hydrolysis products of spiro-diol **3** after storage in a mixture of 0.3 mL CD_3CN and 0.1 mL 10 mM TFA in D_2O after various time intervals at 20 °C. Red arrows indicate the disappearance of the monitored spiro-diol signal and green arrows point out the growth of the characteristic diketone **1** signal. Blue and orange arrows mark the appearance of signals from TMP **2** and diketone **1**, respectively.

SEC traces

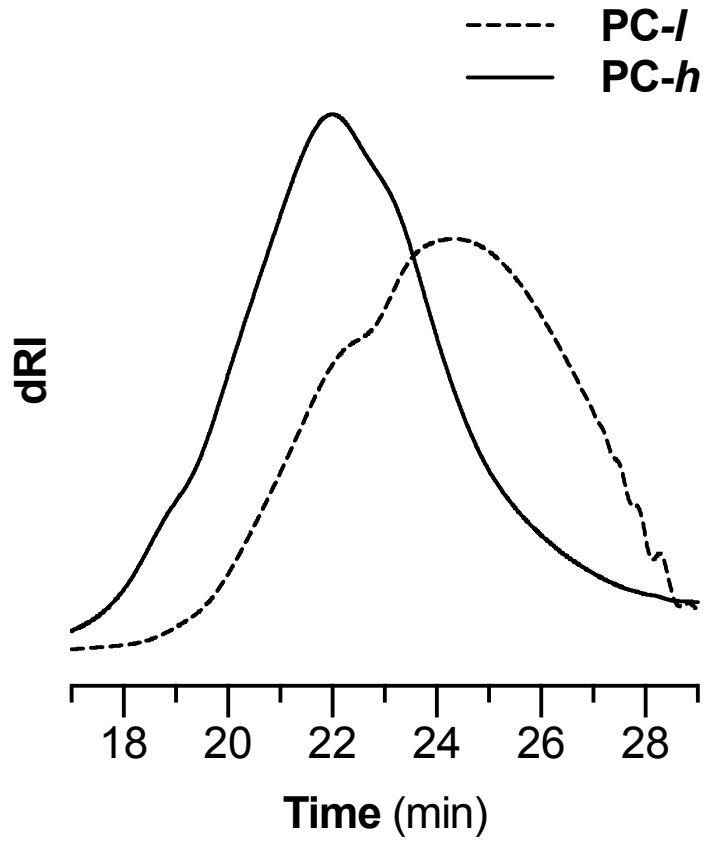

Figure S12. SEC traces of **PC-*l*** and **PC-*h*** in THF recorded by a differential refractive index (dRI) detector.

Optical transmission of PC-*h*

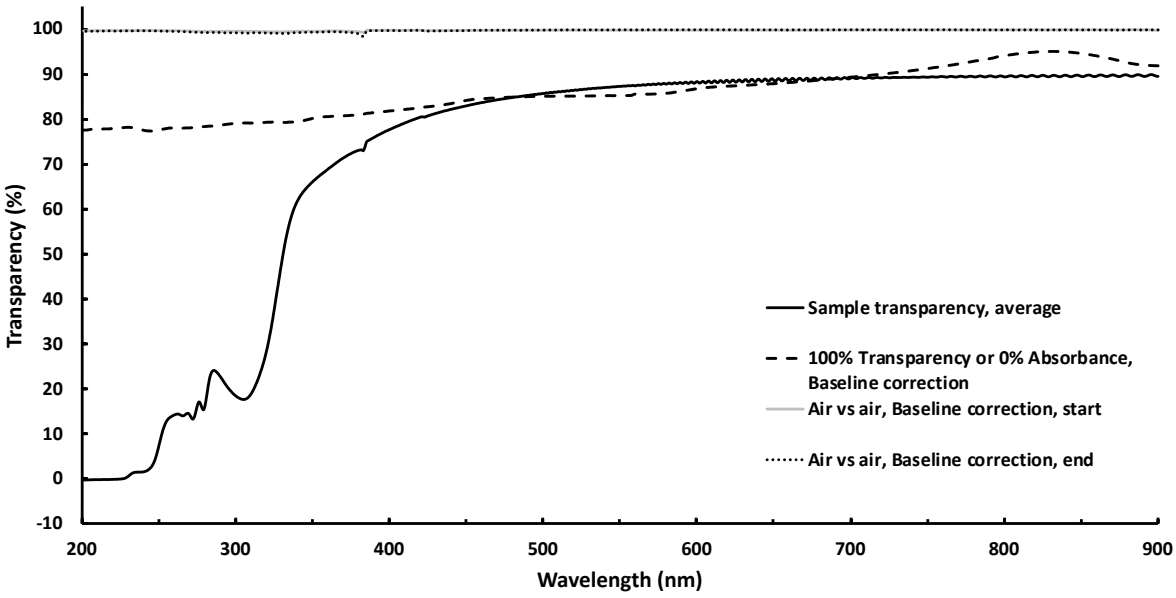

Figure S13. Optical transmission of PC-*h* measured on a 32 μm thick film.

Photograph of a PC-*h* film under mechanical stress

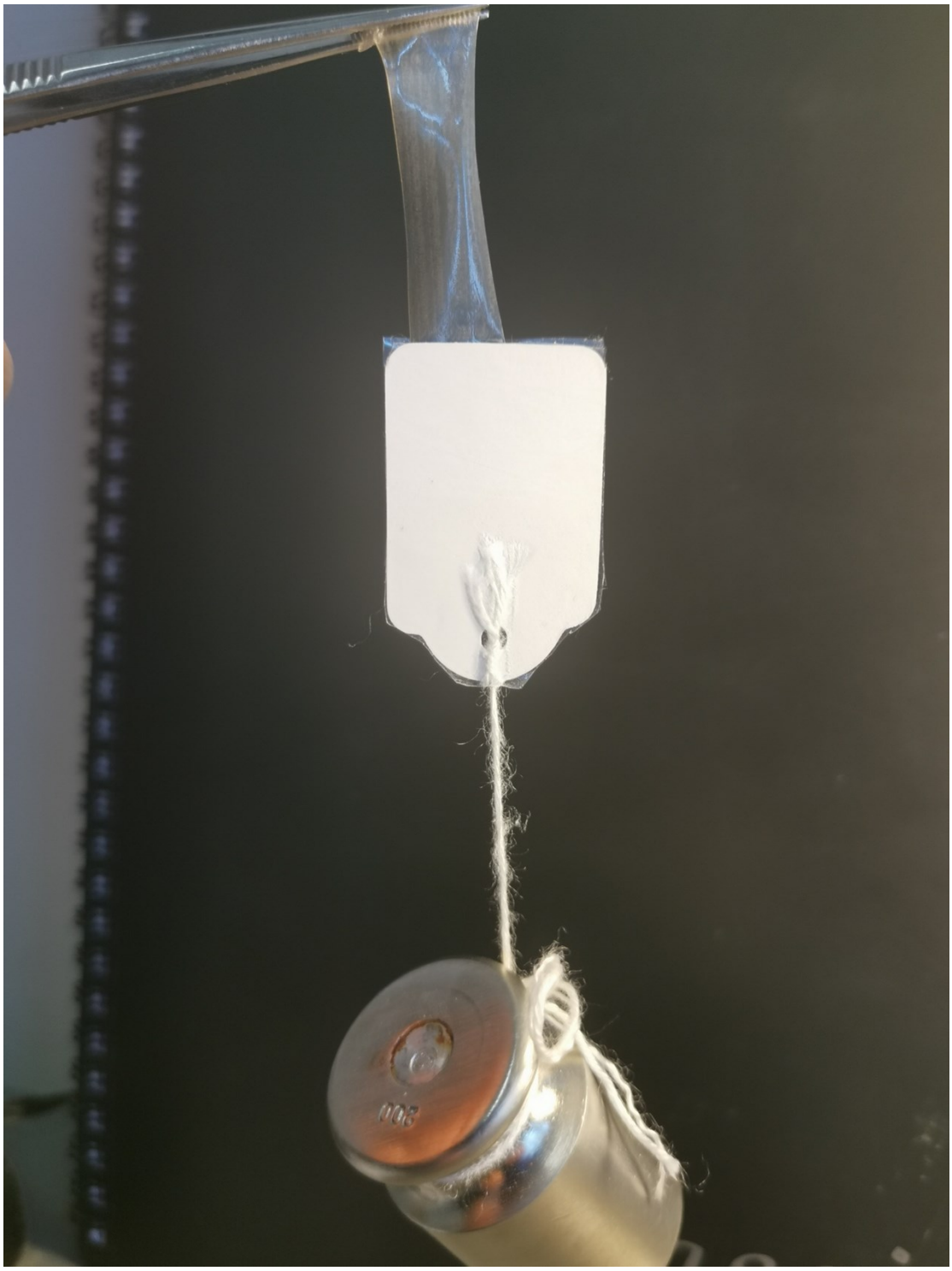

Figure S14. Photograph illustrating the viscoelastic behaviour of a PC-*h* film under mechanical stress (film dimensions: width 8 mm, thickness 55 μm; weight applied: 200 g).